SEVENTH FRAMEWORK PROGRAMME

REDOX PHENOMENA CONTROLLING SYSTEMS
ReCosy
Grant agreement N°.: FP7-212287

COLLABORATIVE PROJECT (CP)

Deliverable D5.2
Redox processes in radionuclide transport in clay rock
(Final report)

CEA

Authors: S. Savoye, A. Fayette, B. Grenut, M. Schlegel, Th. Vercouter

Submitting organizations: CEA
Due date of deliverable: 45 Project Months
Actual submission: 45 Project Months

Start date of the project: 01 April 2008
Duration: 48 months

Project co-funded by the European Commission under the Seventh Framework Programme of the European Atomic Energy Community (Euratom) for nuclear research and training activities (2007 to 2011)		
Dissemination Level		
PU	Public	X
RE	Restricted to a group specified by the partners of the project	
CO	Confidential, only for partners of the project	

1. Introduction

Due to extreme hydraulic and retention properties, indurated clay rocks are considered worldwide as potential host rocks for radioactive waste disposal. Numerous studies have shown that migration of radionuclides in argillaceous rocks is mainly controlled by molecular diffusion. This is the case for the Callovo-Oxfordian claystones (COx). Diffusive parameters of different radionuclides through the COx have been already determined (Descostes *et al.*, 2008; Savoye *et al.*, 2010, 2011, 2012). One can distinguish three different families according to their mobility. Hence, HTO is often taken as an inert tracer since this radiotracer offers the possibility to access to the total porosity. Second, cationic species which are known to be sorbed onto clayey materials, exhibit, however, high effective diffusion coefficient (D_e) compared to neutral species (Gimmi and Kozakoswki, 2010; Savoye *et al.*, 2012). This behaviour, called "surface diffusion mechanism", is attributed the migration of cations within the electrical double layer, next to mineral surfaces. Last, the anionic species migration, such as Cl^-, I^- and Se, as SeO_3^{2-} or SeO_4^{2-}, is characterized by a systematic delay with respect to HTO (Descostes *et al.*, 2009; Savoye *et al.*, 2011, Wittebroodt *et al.*, 2012). This is due to anionic exclusion, as anions are repelled by the permanent negative charge of the surface of clay minerals. However, anions are less subject to sorption onto clayey minerals. This is why $^{36}Cl^-$, $^{129}I^-$ and ^{79}Se are identified among the largest contributors to the performance assessment associated with radioactive waste disposal (Altmann, 2008; Grambow, 2008).

I^- sorption is still under debate (Tournassat *et al.*, 2007; Claret *et al.*, 2010; Wittebroodt *et al.*, 2012). I speciation/redox change may occur during any experiment since generally no special care is taken regarding the speciation. In this case, the formation of IO_3^- may occur. Furthermore, the redox state of argillite may play also a major role as the COx argillite is known for its reducing conditions (Gaucher *et al.*, 2004). Hence, it was shown that I- uptake is strongly dependant on the anoxic conditions (Bazer-Bachi *et al.*, 2006). Concurrently, a weak I^- sorption may also be an artefact since IO_3^- could be sorbed and reduced into I_2 at the FeS_2 surface whereas no sorption of I^- was found (Fuhrmann *et al.*, 1998) Last, a rapid reduction of IO_3^- into I^- was observed during a diffusion test through the Opalinus Clay (OPA) (Glaus *et al.*, 2008). The same question arises with selenium, especially for Se(+IV), i.e. SeO_3^{2-}. Even though SeO_3^{2-} sorption onto clayey minerals was previously reported (Jacquier *et al.*, 2001), one may wonder if its sorption occurs without redox change as underlined by the very low D_e measured in COx (Descostes *et al.*, 2008) and its reduction observed onto FeS_2 surface (Bruggeman *et al.*, 2005). To our knowledge, diffusive data regarding SeO_4^{2-} in hard clay rocks are only available for the Boom clay formation (De Cannière *et al.*, 2010). In this case, the diffusive parameters for SeO_4^{2-} are very close to those of SO_4^{2-}.

One may extend the definition of anionic species in the frame of migration of actinides in hard clay rocks from a deep geological waste disposal. The high sulphate and carbonate contents in porewaters drastically change the speciation of actinides since from cationic form as predicted in pure water whatever their oxidation number, they become mainly under anionic species as CO_3^{2-} and SO_4^{2-} complexes. The diffusive behaviour of such oxyanions of high molecular weight in hard clay rocks may differ from halides. Besides, redox transformations may also occur during interaction between argillite and actinides as illustrated by the reduction of U(VI) observed on FeS_2 surface (Aubriet *et al.*, 2006).

This study aimed at understanding the diffusive behaviour of redox-sensitive anions (I, Se) and oxyanions of high molecular weight (U) in the COx argillite. The main challenge was to exclude as much as possible the occurrence of any experimental artefact that could induce

phenomena (oxygen contamination, dissolution/precipitation of carbonate phases) that would not prevail in-situ. Therefore, all the experiments were carried out under physico-chemical conditions as close as possible to those prevailing in field, from the sample preparation until the dismantling of the experiments. Using a glove box with an atmosphere of N_2/CO_2 (respectively 99.6% and 0.4%), we preserved the experiments from oxygen and maintained the calculated in-situ carbonate equilibrium. Moreover, a special attention was paid for monitoring any change of the iodine and selenium redox state throughout the duration of the experiments.

2. Materials and Methods

2.1. Sample Origin and Sample Preparation

The rock core used for the measurements was collected from the borehole OHZ1202 (X= 823252 m; Y= 1091659.37m; Z= -115.54 m NGF), argon-drilled upwards in the Meuse/Haute Marne Underground Laboratory, located in the eastern portion of the Paris basin. The sedimentary host formation (152-160 Ma) is a ~130-m-thick clay-rich Callovo-Oxfordian formation and with a burial depth of ~420-550 m below ground level (bgl). According to Gaucher *et al.*(2004), the level from which the core originates (EST30471 core 480.7-481.7 m bgl) corresponds to silty and calcareous argillites, containing 35-65% of clay minerals (with 27-38% of mixed layer Illite/smectite), 15-28% of carbonates, 21-31% of quartz, and accessory minerals. Six samples were sliced from the EST30471 claystone core using a diamond wire saw (no lubricating fluid was used) into 1-cm-thick pieces under anoxic conditions (O_2 < 5 ppm). Then nine were cut as a disk (ϕ ~ 38 mm) for the diffusion experiments and two were powdered for the batch (particle size < 63 µm).

2.2. Analytical procedure to estimate the fraction of $^{125}I^-$ and of $^{125}IO_3^-$, or $^{75}SeO_3^{2-}$ and $^{75}SeO_4^{2-}$

The principle to derive the iodine and selenium speciation was based on an ion chromatography separation stage followed by a gamma counting of the different fractions (see Glaus *et al.*, 2008 for details). The high-performance anion exchange chromatography system was a Metrohm 761 Compact IC (Metrohm, Switzerland) with a 50 µL injection loop and a 500 µL sample syringe. The separation of iodide and iodate, or selenite and selenate was performed on an 4 x 250 mm A-Sup5 column (Metrohm, Switzerland) using an elution of 3.5 mmol L^{-1} $NaHCO_3$/ Na_2CO_3 at a flow of 0.7 and 0.6 cm^3 min^{-1} for iodine and selenium, respectively. Elution of the analytes was monitored in the conductivity mode.

In order to determine the times during which $^{125}I^-$ and of $^{125}IO_3^-$ or $^{75}SeO_3^{2-}$ and $^{75}SeO_4^{2-}$ fractions had to be collected, aqueous standards of stable iodide and iodate, or selenite and selenate at a concentration of 10^{-3} mol L^{-1} were eluted and monitored by conductivity.

2.3. Synthetic pore-water composition

Solutions were prepared with ultrapure deionised water (18.2 MΩ cm^{-1}) and commercial salts (American Chemical Society (ACS) reagent grade or higher quality and purity salts) in order to obtain a chemical composition as close as possible to the pore-water one. The recipe given in Table 1 is based upon the chemical composition estimated from *in situ* water sampling performed at a level close to the sampling level of this study (-475m bgl; Vinsot *et al.*, 2007). The CO_2 content of the glove box (0.4% CO_2 for 99.6% N_2) was chosen close to the in-situ Callovo-Oxfordian claystone CO_2 partial pressure (i) to preserve as much as possible the equilibrium with carbonate minerals (Vinsot *et al.*, 2007; Beaucaire *et al.*, 2008)

and (ii) to avoid any co-precipitation of iodide with carbonates, as already mentioned by Claret *et al.* (2010).

Table 1: *Composition of synthetic water used in this study*

$[Cl^-]$ (mmol L^{-1})	$[SO_4^{2-}]$ (mmol L^{-1})	ΣCO_2 (mmol L^{-1})	$[Na^+]$ (mmol L^{-1})	$[K^+]$ (mmol L^{-1})	$[Ca^{2+}]$ (mmol L^{-1})	$[Mg^{2+}]$ (mmol L^{-1})
41.00	15.6	2.57	51.9	1.04	6.44	4.48

2.4 Batch experiments for iodine and selenium series

About 1.2 g or 0.4 g (I or Se, respectively) of argillite powder (particle size < 63 µm) was put into 10 mL centrifugation tube (#NALGENE PC 31-38-0010, USA). The synthetic pore-water was added to tubes with Water/Rock (W/R) value of 4 or 18 mL g^{-1} (I or Se, respectively). All the experiments were carried out in an oxygen-depleted (<5 ppm O_2) glove box with a 99.6% N_2/0.4% CO_2 atmosphere and operated at ambient temperature (21 ± 1 °C).

According to Descostes and Tevissen (2004), the equilibration phase started by a first step of 72h of equilibration followed by two rinsings lasted one week each. Iodide or selenite tracers were added after equilibration as $^{125}I^-$ (#CERCA I125ELSB50, France) or as $^{75}SeO_3^{2-}$ (Eckert & Ziegler, Germany) with variable concentration of stable iodide (NaI, Fluka, Switzerland) or stable selenite (Na_2SeO_3, Fluka, Switzerland) to reach a range of total iodine or selenite concentration varying between 10^{-6} to 10^{-3} mol L^{-1}. Two duplicates were used for each concentration. As already mentioned by De Cannière *et al.* (2010), most of the ^{75}Se(+IV) sources supplied by the manufacturers were accompanied by Se(+VI), because of the water radiolysis of the ^{75}Se stock solution. Therefore, using the ionic chromatography method as described above (§2.2.), we determined that 5.3% of the ^{75}Se stock was under selenate form. Sorption was investigated for 106 days and 125 days (I and Se, respectively) by successive samplings in each tube. Before sampling, tubes were centrifuged at 96,000 g for 45 min. Supernatant (50 µL) was then withdrawn, weighted and analysed by gamma counting (Packard 1480 WIZARD, USA). Blank experiments did not reveal any sorption for iodide, while for selenite, the blank experiment carried out at the lowest concentration (10^{-6} mol L^{-1}) exhibited a drop of the ^{75}Se, related to a possible bacteria-enhanced reduction, making difficult any interpretation of this series. At the end of the batch experiment, the same procedure described above was applied, except the filtration of supernatants at 0.2 µm.

The distribution ratio R_D (L kg^{-1} or mL g^{-1}) was calculated using the following equation:

$$R_D = \frac{C_0 - C}{C_0} \times \frac{W}{R} \qquad (1)$$

Where C_0 is the initial activity per volume unit (kBq L^{-1}); C the residual activity in solution per volume unit (kBq L^{-1}); W the solution volume (L) and R the dry mass of argillite (kg). Note that the solution volume (W) was recalculated after each withdrawn to take into account the change of water/rock ratio into Eq. (1).

2.5. Diffusion experiments

2.5.1. Equipment

Figure 1 schematically represents the diffusion cells used in this study. The through-diffusion cells comprise two reservoirs in polypropylene (up and downstream: 175 and 130 mL, respectively), a polypropylene sample holder, two holed plates in polyetheretherketone

(Peek), the whole being pasted with glue and screwed together. Each part of the diffusion cell was beforehand cleaned with HNO_3 (1%) and water, and dried. All the preparation of the diffusion cells was made in a glove box (O_2 < 5 ppm). As for the batch experiments, all of the ones dedicated to diffusion were carried out in a glove box with a 99.6% N_2/0.4% CO_2 gas mixture and operated at ambient temperature (21 ± 1 °C).

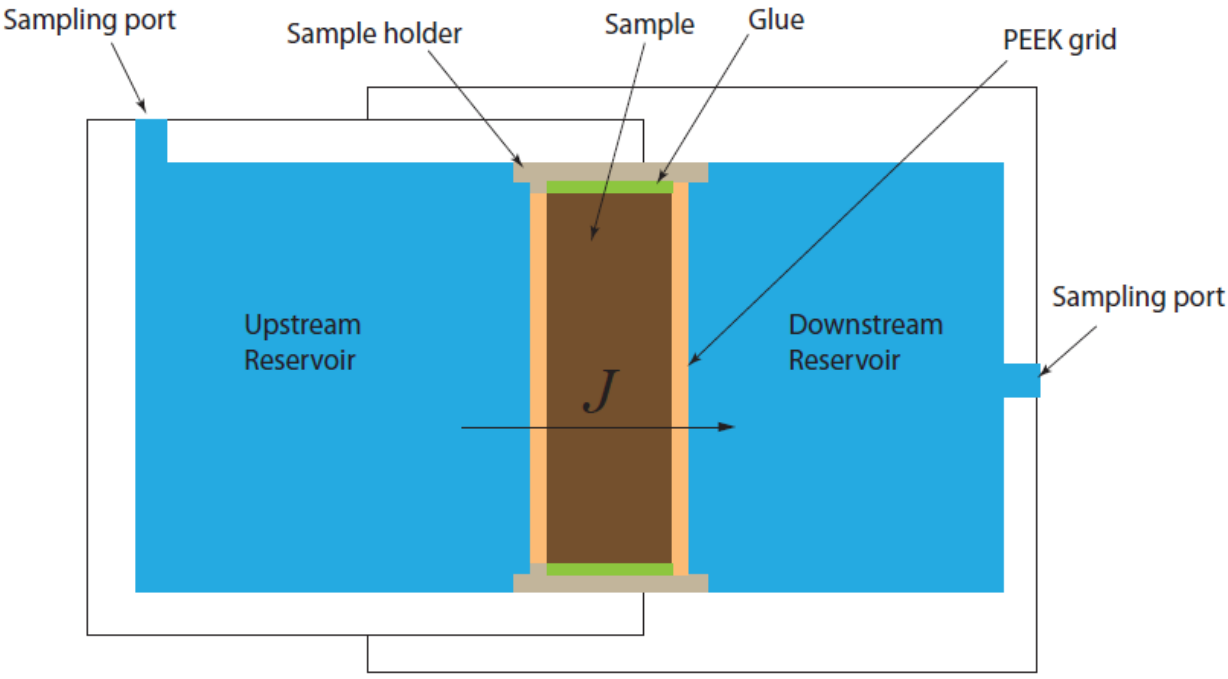

Figure 1: *Experimental set-up for through diffusion experiment*

2.5.2. Protocols

Table 2 gives an overview of the nine cells used for investigating diffusion. Seven were used with radioactive tracers (^{125}I and ^{75}Se), while the two others were used with stable selenite or uranium.

Diffusion cells used with radioactive tracers

The rock disks in the seven diffusion cells were equilibrated over at least 4 weeks, with the synthetic solution of the composition given by Table 1. This time was found to be sufficient to reach chemical equilibrium (Motellier *et al*., 2007; Savoye *et al*., 2010; Savoye *et al*., 2011). Note that for iodide series, among the five diffusion cells, one had the chemical composition of its synthetic solution modified by adding $Na_2S_2O_3$ (Fluka, Switzerland) at 10^{-3} mol L^{-1}. The objective was to investigate the effect of a reductive agent – the thiosulfate- capable of consuming the oxygen traces occurring in the glove box, in order to limit the oxidation of the rock sample, and especially the pyrite in more reactive minerals towards iodine (Aimoz *et al.*, 2011). This operation was previously performed by Bazer-Bachi *et al.* (2006) and Descostes *et al.* (2008) on COx samples but under oxic conditions.

Table 2: *Overview of the tracers used and their initial activity, and the type of diffusion experiments performed. n-d: not determined.*

Cells	HTO/^{36}Cl through-diffusion MBq L^{-1}	^{125}I, ^{75}Se or U(+VI) diffusion	out-diffusion or Rock profile	new through-diffusion
EST30471-1 Iodide	HTO 3.68±0.22 ^{36}Cl 4.30±0.24	5.02 MBq L^{-1} +[I$^-$]= 10^{-3} mol.L^{-1}	Out-diff	n-d
EST30471-2 Iodide	HTO 3.68±0.22 ^{36}Cl 4.30±0.24	4.88 MBq L^{-1} +[I$^-$]= 10^{-4} mol.L^{-1}	Out-diff	n-d
EST30471-3 Iodide	HTO 3.68±0.22 ^{36}Cl 4.30±0.24	5.02 MBq L^{-1} +[I$^-$]= 10^{-5} mol.L^{-1}	Out-diff	n-d
EST30471-4 Iodide	HTO 3.68±0.22 ^{36}Cl 4.30±0.24	4.89 MBq L^{-1} +[I$^-$]= 10^{-6} mol.L^{-1}	Out-diff	4.24 MBq L^{-1} +[I$^-$]= 10^{-3} Mol.L^{-1}
EST30471-5 Iodide + [NaS_2O_3]= 10^{-3} mol L^{-1}	HTO 4.53±0.05 ^{36}Cl 5.16±0.05	2.94 MBq L^{-1} +[I$^-$]= 10^{-6} mol.L^{-1}	Out-diff	n-d
EST30471-6 Selenium	HTO 4.6±0.3 ^{36}Cl 5.2±0.3	5.00 MBq L^{-1} [Se(4)]= 10^{-3} mol L^{-1}	Rock-profile = µabrasion	n-d
EST30471-7 Selenium	HTO 4.6±0.3 ^{36}Cl 5.2±0.3	5.00 MBq L^{-1} [Se(4)]= 10^{-6} mol L^{-1}	Rock-profile = µabrasion	n-d
EST30471-8 Selenium	n-d	[Se(4)]= 2 x 10^{-3} mol L^{-1}	Rock-profile = XAS	n-d
EST30471-9 Uranium	n-d	[U(6)]= 3 x 10^{-6} mol L^{-1}	n-d	n-d

Subsequently the solution was replaced by a fresh one. First of all, the solution in the upstream reservoir was spiked with HTO, a water tracer and ^{36}Cl (see Table 2 for the injected activities). Both compartments were periodically sampled, the solution volume being renewed in each compartment either by the radiolabelled solution or by the synthetic water. The monitoring of the ^{36}Cl flux through the rock sample allows the determination of the diffusion-accessible porosity of a non-reactive anionic tracer (ε_a). After completion of the first through-diffusion stage, an out-diffusion procedure was applied to the seven cells. So, the solutions in both reservoirs were replaced by synthetic solution without tracer to make HTO and ^{36}Cl diffuse out of the rock samples. At selected time intervals, the activity in the solutions was measured just before replacing them by fresh ones. This procedure was repeated until the activity measurement led to values close to the background activity values. Then, a second through-diffusion stage was performed by introducing into the upstream reservoir, both stable dissolved iodide (NaI, Fluka, Switzerland) at a concentration ranging

from 10^{-3} mol L^{-1} to 10^{-6} mol L^{-1} and the ^{125}I-labelled source (#CERCA I125ELSB50, France) or stable dissolved selenite (Na_2SeO_3, Fluka, Switzerland) at two concentrations (10^{-3} mol L^{-1} and 10^{-6} mol L^{-1}), and the ^{75}Se-labelled source Eckert & Ziegler, Germany) (Table 2). Note that the presence of 5.3% of $^{75}SeO_4^{2-}$ in the radioactive source (see above) enabled us to perform a double spike with on one hand, stable and radioactive Se(+IV) and, on other hand, only radioactive Se(+VI). In addition to the regular sampling used for monitoring the ^{125}I or ^{75}Se activity evolution, 2 mL of solutions were withdrawn throughout the diffusion stage in order to monitor any changes of the iodide or selenium speciation with the help of the ionic chromatography separation (§ 2.2.).

After the iodide through-diffusion stage (210 days), a new out-diffusion procedure was carried out to study the behaviour of the iodide diffusing out of the rock sample. Besides, the cell in which was injected iodide at a concentration of 10^{-6} mol L^{-1} without $Na_2S_2O_3$ underwent a new through-diffusion stage with iodide injected at a concentration of 10^{-3} mol L^{-1}. This allowed us to test the effect of iodide initial concentration on its retention behaviour towards the same rock sample, overcoming the mineralogical heterogeneity issue.

After 240 days of selenium diffusion, the two cells were dismantled by removing the sample holders from these cells. The sample holders were roughly dried overnight in the dried atmosphere of the glove box, and afterwards in an oven at 70°C, out of the glove box, for 3 days. Then, the abrasive peeling technique developed by Van Loon and Eikenberg (2005) for Opalinus Clay, was applied to the two rock samples, previously extracted from the sample holder and the glue. This technique enables the abrasion of a sample layer, thickness of which can vary from 10µm to 250 µm depending of the abrasion duration and the type of the grit grinding paper used (from P220 to P80). The choice of the thickness is directly related to the distance to the disk surface previously in contact with the upstream reservoir solution. That means that the closer to the disk surface the layer, the higher the specific ^{75}Se activity and the smaller the thickness. The ^{75}Se activity in the abraded layers was measured by χ-spectroscopy.

Diffusion cells used with stable Selenite or Uranium

Only an in-diffusion stage was carried out for selenium, directly after the equilibration stage, by introducing stable dissolved selenite (Na_2SeO_3, Fluka) at a concentration of 2 x 10^{-3} mol L^{-1} into the upstream reservoir. This concentration value was chosen to be under the solubility limit of $CaSeO_3$ (Baur and Johnson, 2003), but sufficiently high so as to allow selenium detection by spectroscopic analysis. A regular sampling was performed for monitoring the decrease of the selenite concentration in solution. Analyses of stable selenite concentration were performed by ion exchange chromatography with an accuracy of about 7%. This analytical technique also allowed the identification of selenate, if any.

After 508 days of selenium diffusion, the cell was dismantled and the rock sample was dried in the anhydrous atmosphere of an O_2-free glove box for 3 days, and then cut into a 2mm-thick section. The oxygen contamination was limited as much as possible (i) during the transportation to the synchrotron facility by using an air-tight tank and (ii) during the XAS analyses by inserting the sample into a vacuum chamber (~5 10^{-4} mBar). Selenium K-edge X-ray Absorption Near-Edge Structure (XANES) and Extended X-ray Absorption Fine-Structure (EXAFS) spectra were collected at the Synchrotron Laboratory for Environmental Studies (Synchrotron Umwelt-Labor SUL) at ANKA (Karlsruhe, Germany).

Through-diffusion experiment with U(+VI) injected at a concentration of 3 10^{-6} mol L^{-1} was also carried out for 400 days. Time-resolved laser-induced fluorescence spectroscopy method (TRLFS) was performed regularly on the upstream solution for estimating the speciation of the Uranium.

Submitting organizations: CEA
Due date of deliverable: 45 Project Months
Actual submission: 45 Project Months
Grant agreement N°.: FP7-212287
Start date of the project: 01 April 2008
Duration: 48 months
Project co-funded by the European Commission under the Seventh Framework Programme of the European Atomic Energy Community (Euratom) for nuclear research and training activities (2007 to 2011)

Dissemination Level		
PU	Public	X
RE	Restricted to a group specified by the partners of the project	
CO	Confidential, only for partners of the project	

2.5.3. Data analysis

The analysis of the results was based on Fick's second law for one-dimensional reactive transport:

$$\frac{\partial C}{\partial t} = D_a \frac{\partial^2 C}{\partial x^2} = \frac{D_e}{\alpha}\frac{\partial^2 C}{\partial x^2} = \frac{D_e}{\varepsilon_a + \rho R_D}\frac{\partial^2 C}{\partial x^2} \quad (2)$$

Where C is the is concentration or activity per volume unit (mol m^{-3} or Bq m^{-3}); t, the time (s); D_a, the apparent diffusion coefficient (m^2 s^{-1}); D_e, the effective diffusion coefficient ($m^2.s^{-1}$); α, the rock capacity factor; ε_a, the diffusion-accessible porosity; ρ, the bulk dry density (kg m^{-3}) equal to 2.35 kg m^{-3} for the COx (Savoye *et al.*, 2011); and R_D, the distribution ratio (m^3 kg^{-1}).

According to van Brakel and Heertjes (1974), D_e can be written as follows:

$$D_e = D_p \varepsilon_a = \frac{\delta}{\tau^2} D_0 \varepsilon_a = \frac{D_0}{G}\varepsilon_a \quad (3)$$

Where D_0 is the free-solution (aqueous) diffusion coefficient ($m^2.s^{-1}$), δ represents the constrictivity factor (-), and τ is the tortuosity factor. G is the geometrical factor. Tortuosity and constrictivity are purely geometric factors, which, compared with a specific cross-section in free water, lengthen the diffusion pathway and reduce the diffusion cross-section, respectively (van Brakel and Heertjes, 1974).

For the through diffusion problem, the boundary and initial conditions are given by:

$C(x, t) = 0, \quad t = 0$ (4)

$C(x, t) = C_0, \quad x = 0, t > 0$ (5)

$C(x, t) = 0, \quad x = L, t > 0$ (6)

Where L is the sample thickness (m), and C_0 is the concentration of the tracer in the upstream reservoir (Bq m^{-3}). For HTO and ^{36}Cl, which are non reactive tracers ($R_D = 0$), α is equal to ε_a. The solution of Eq. (2), satisfying the boundary and initial conditions was given by Crank (1975), as the diffusive flux (Bq m^{-2} s^{-1}) in the downstream reservoir:

$$J(t) = D_e \frac{C_0}{L}\left[1 + 2\sum_{n=1}^{\infty}(-1)^n \exp\left(\frac{-D_e n^2 \pi^2 t}{\varepsilon_a L^2}\right)\right] \quad (7)$$

For the out-diffusion stage, Eq. (2) has to be solved with the corresponding boundary conditions:

$C(0,t)=C(L,t)=0; \; t>0$ (8)

Assuming that the concentration gradient across the sample is linear when the through-diffusion stage reaches the steady-state, the concentration profile that gives the initial conditions for out-diffusion, is:

$$C(x) = C_0\left(1 - \frac{x}{L}\right) \quad (9)$$

According to Jakob *et al.* (1999), the total activity (Bq) diffused out of the sample at the two boundaries is given:

At x = 0: $$A(0,t) = 2 \cdot C_0 \cdot S \cdot \alpha \cdot L\left[\frac{1}{6} - \sum_{n=1}^{\infty}\frac{1}{\pi^2 n^2} e^{-\left(\frac{n\cdot\pi}{L}\right)^2 \cdot \frac{D_e}{\alpha}\cdot t}\right] \quad (10)$$

And

At x = L: $$A(L,t) = 2 \cdot C_0 \cdot S \cdot \alpha \cdot L \left[\frac{1}{12} + \sum_{n=1}^{\infty} \frac{(-1)^n}{\pi^2 n^2} \cdot e^{-\left(\frac{n \cdot \pi}{L}\right)^2 \cdot \frac{D_e}{\alpha} \cdot t} \right] \quad (11)$$

Where *S* is the surface of the rock sample (m^2).

For modelling the selenium in-diffusion data, a single reservoir method with decreasing source concentration for a semi-infinite case was used (Shackelford, 1991). The initial and boundary conditions are as follows:

$C(x \leq 0, t=0) = C_0, \quad C(x>0, t=0) = 0 \quad (12)$

$$\frac{\partial C(x=0, t>0)}{\partial t} = -\frac{D_e \alpha}{H_f \varepsilon_a} \frac{\partial C(x=0, t>0)}{\partial x} \quad (13)$$

$C(x=\infty, t>0) = 0 \quad (14)$

where the positive x-direction corresponds to the solid and H_f is the length of upstream reservoir (m). ε_a is the porosity accessible to a non reactive anionic species, *i.e* ^{36}Cl, and α is the rock capacity factor determined for the selenite.
An analytical solution for these initial and boundary conditions is (Shackelford, 1991):

$$\frac{C(x,t)}{C_0} = \exp\left[\frac{\alpha x}{H_f} + \frac{\alpha D_e t}{H_f^2} \right] \times erfc\left(\frac{x}{2\sqrt{D_e t / \alpha}} + \frac{\sqrt{D_e \alpha t}}{H_f} \right) \quad (15)$$

Where *C(x,t)* the concentration of the tracer in the pore water of the rock at distance *x* after time *t* (Bq m^3 or mol m^{-3}), and erfc(*z*) is the complementary error function of argument *z*.

The analysis of the results was performed by a least-square fitting of the model to the results of (i) the incoming daily flux in the downstream reservoir for through-diffusion, (ii) the cumulative total activities in the downstream and the upstream reservoirs, and the decrease of activity in the upstream reservoir and the rock profile activity, using the analytical solutions (Eqs. (7), (10), (11), and (15)).

2.6. Analyses

Activities were counted by α–β liquid scintillation (Packard TRICARB 2500, USA) for HTO and ^{36}Cl and by χ counter (Packard 1480 WIZARD, USA) for ^{125}I and ^{75}Se. The counting efficiency for each tracer was measured using synthetic water with known amounts of radioactivities. Background measurements were performed in a similar way using synthetic water without radiotracers. HTO-, ^{36}Cl-, and $^{125}I^-$ solution data were corrected for radioactive decay with respect to the tracer injection time, i.e., the start of the through-diffusion experiment. ^{75}Se solution data were corrected for radioactive decay with respect to the tracer injection time, while ^{75}Se rock profile data were corrected with respect to the dismantling time.The Uranium concentration was determined by ICP-MS (Varian, Agilent Technologies, USA).

3. Results

3.1. Iodide case

3.1.1. Iodine redox-state

The determination of the iodine redox-state was carried out (i) in the initial ^{125}I source, (ii) in the upstream reservoir solutions during the through diffusion experiments after 112 days, 196 days and at the end of the through-diffusion stage, and (iii) in the blank used in the batch. No significant activity (less than 0.1 Bq) was measured in all the fractions expected to contain $^{125}IO_3^-$. Moreover, the $^{125}I^-$ fractions showed activity values very close to those measured in the corresponding overall solutions with a standard deviation of 2% (5 samples).

3.1.2. Batch experiments

Figure 2 displays the evolution as a function of time of the R_D values obtained at the four initial iodide concentrations on the Callovo-Oxfordian (COx) claystone duplicates. Whatever the concentration, the R_D values did not exhibit any increase with time but only a large scattering, from which no ^{125}I sorption can be evidenced, even after 106 days of contact time.

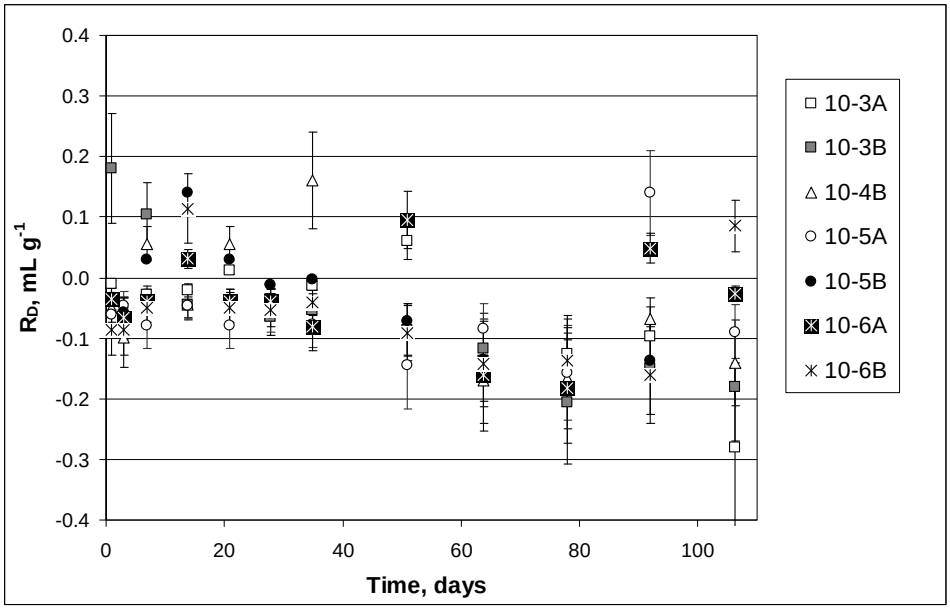

Figure 2: *Evolution as a function of time of the distribution ratio (R_D) values derived from batch experiments. The series 10-4A was removed because of a problem of a solution leakage.*

3.1.3. Diffusion results

Through-diffusion stage

Figure 3 shows an example of the instantaneous fluxes and the cumulative total activities obtained on the cell EST30471-1 for HTO (A), ^{36}Cl (B), and ^{125}I with an initial iodide concentration at 10^{-3} mol L^{-1} (C). All the diffusive parameters estimated from the through-diffusion stage were gathered in the Table 3 for HTO and ^{36}Cl and in the Table 4 for ^{125}I. The values of the effective diffusion coefficient and the porosity for HTO and ^{36}Cl were quite consistent each other ($<D_e(HTO)>=2.84\pm0.37 \times 10^{-11}$ m² s^{-1}; $<\varepsilon(HTO)> = 0.20\pm0.02$; $<D_e(^{36}Cl)>=0.42\pm0.13 \times 10^{-11}$ m² s^{-1}; $<\varepsilon(^{36}Cl)> = 0.086\pm0.015$). They were also in good agreement with those previously obtained by Descostes *et al.*(2008) and Savoye *et al.*(2010)

on nearby samples (less than 4 m away) but they were slightly lower than those from Bazer-Bachi *et al.*(2006) on samples located about 30 m above (see Table 3 for comparison).
The values of the effective diffusion coefficient obtained in the current study for ^{125}I were very close to those for ^{36}Cl with a mean $D_e(^{125}I)$ equal to 0.47±0.17 x 10^{-11} m² s^{-1}, also consistent with the values previously obtained by Bazer-Bachi *et al.*(2006), Descostes *et al.*(2008), and Savoye *et al.*(2010). Moreover, only when the initial iodide concentration injected in the cells was less than or equal to 10^{-4} mol L^{-1}, the rock formation factor – α- became higher than the porosity accessible to ^{36}Cl (Table 3 and Table 4). This led to estimate weak but significant values of R_D (~0.05 mL g^{-1}), in agreement with what observed Bazer-Bachi *et al.*(2006) on COx samples (see Table 4). Note that, contrary to the Bazer-Bachi *et al.*'s study, the porosity accessible to a non-reactive anionic species, i.e., $^{36}Cl^-$, was systematically determined on each sample for which the iodide through-diffusion was carried out. Therefore, this prevents any suspicion from arising about the possible role played by the mineralogical heterogeneity on the apparent iodide retardation (e.g., local increase of the ^{36}Cl porosity). Moreover, the issue of the mineralogical heterogeneity was also addressed by performing on the same rock sample (cell EST30471-4), two successive injections of iodide at 10^{-6} mol L^{-1} and 10^{-3} mol L^{-1}.

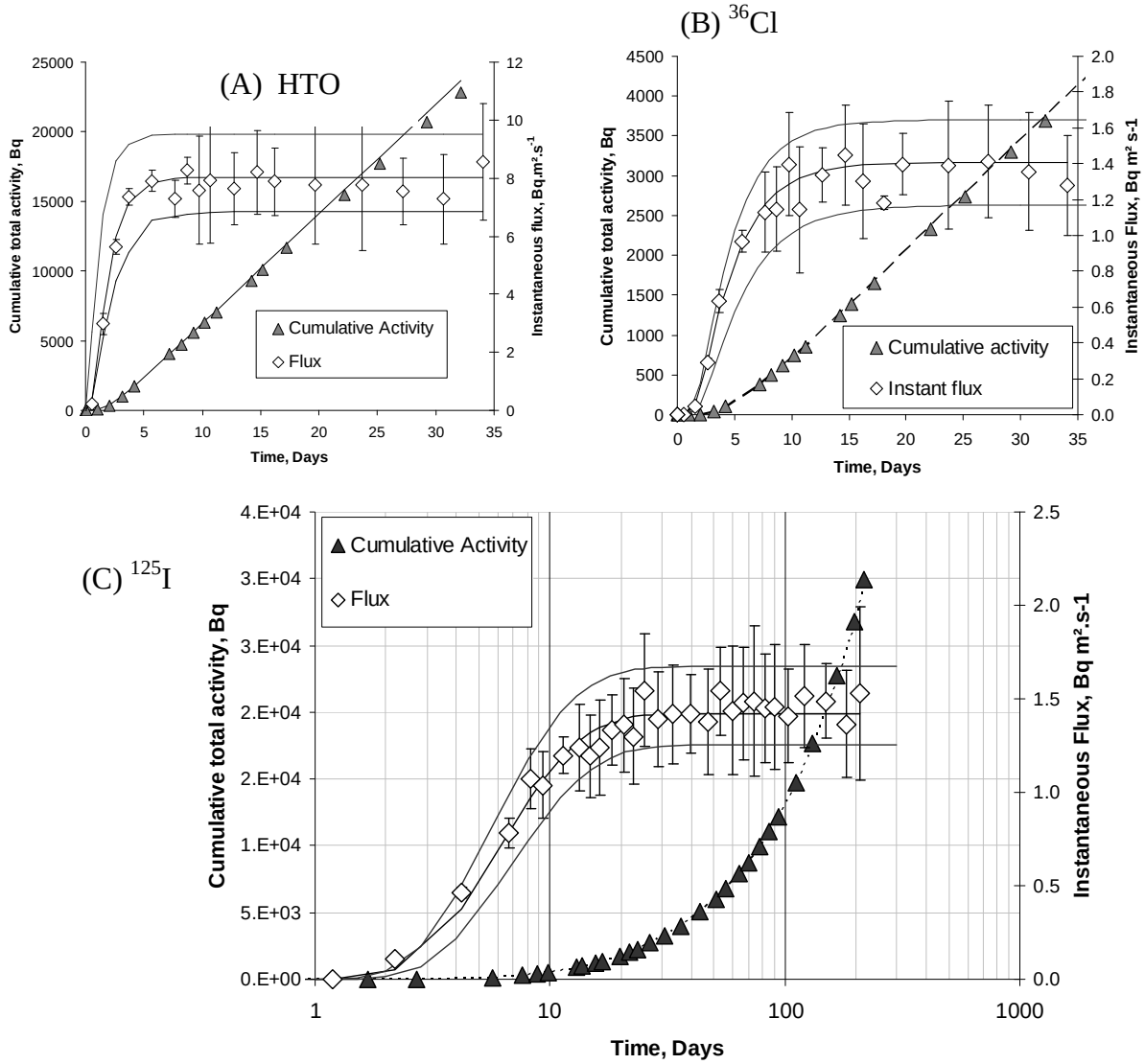

Figure 3: *Cumulative total activity and instantaneous flux obtained on the cell EST30471-1 for HTO (A), ^{36}Cl (B), and ^{125}I with $[I^-]_{ini} = 10^{-3}$ mol L^{-1} (C). Curves were obtained from the analytical solutions with the values of diffusive parameters given in Table 3 and Table 4.*

Figure 4 shows the comparison of the normalised fluxes obtained on this cell for ^{36}Cl, and for ^{125}I with the two stable iodide concentrations. The diffusive behaviour of ^{125}I clearly depended on the initial iodide concentration. At 10^{-3} mol L^{-1}, ^{125}I diffused more or less like ^{36}Cl, with a R_D value not significant regarding the uncertainties (Table 4). Conversely, at the lowest concentration, ^{125}I exhibited a significant retardation. Finally, the addition of $Na_2S_2O_3$ in the cell EST30471-5 did not reduce the extent of the iodide retardation (Table 4).

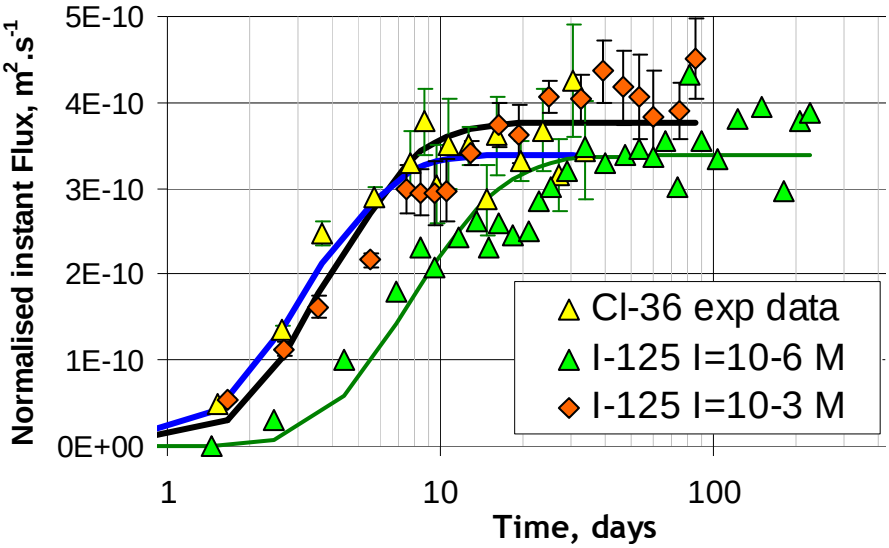

Figure 4: *Comparison of the normalised instantaneous fluxes obtained on the cell EST27321-4 for ^{36}Cl, ^{125}I with $[I]_{ini} = 10^{-6}$ mol L^{-1}, and for ^{125}I with $[I]_{ini} = 10^{-3}$ mol L^{-1}. Grey dashed line corresponds to the simulated curve for $^{36}Cl^-$.*

Table 3: *Effective diffusion coefficients and porosities for the diffusion of HTO and ^{36}Cl through the Callovo-Oxfordian claystones. Values between brackets indicate the uncertainty ranges.*

Cells	HTO		^{36}Cl	
	De x 10^{11} m^2 s^{-1}	Porosity, -	De x 10^{11} m^2 s^{-1}	Porosity, -
EST30471-1 480.7-481.7m	2.7 (2.3-3.2)	0.20 (0.22-0.20)	0.39 (0.32-0.45)	0.07 (0.07-0.09)
EST30471-2 480.7-481.7m	3.2 (3.0-3.6)	0.21 (0.18-0.24)	0.53 (0.46-0.65)	0.10 (0.08-0.12)
EST30471-3 480.7-481.7m	2.65 (2.3-3.0)	0.22 (0.20-0.24)	0.28 (0.22-0.33)	0.10 (0.08-0.11)
EST30471-4 480.7-481.7m	2.4 (1.9-2.8)	0.18 (0.17-0.20)	0.31 (0.27-0.36)	0.07 (0.06-0.08)
EST30471-5 with NaS_2O_3 480.7-481.7m	3.25 (2.9-3.7)	0.17 (0.15-0.20)	0.58 (0.45-0.70)	0.09 (0.08-0.10)
EST27337 [a] 484.5-484.8m	2.3 (1.7-2.85)	0.21 (0.19-0.22)	0.27 (0.2-0.32)	0.075 (0.06-0.085)
EST05641 [b] 476.97-477.35m	2.2±0.7 (3 samples)	0.195±0.045 (3 samples)	0.46	0.065
EST10425 [c] 454 m	2.9±0.1 (5 samples)	0.226±0.017 (5 samples)	0.91	0.168

[a] data from Savoye *et al.*(2010) on PAC1011 core. [b] data from Descostes *et al.*(2008) on EST205 core. [c] data from Bazer-Bachi *et al.*(2006) on EST312 core.

Table 4: *Effective diffusion coefficients, rock capacity factors and distribution ratio for ^{125}I estimated from through- and out-diffusion experiments. Values between brackets indicate the uncertainty ranges. n-d: not determined.*

Cells	Through-diffusion			Out-diffusion from upstream Res.			Out-diffusion from downstream Res.		
	De x 10^{11} m^2 s^{-1}	α, –	R_D x 10^3 mL g^{-1}	*De* x 10^{11} m^2 s^{-1}	α, –	R_D x 10^3 mL g^{-1}	*De* x 10^{11} m^2 s^{-1}	α, –	R_D x 10^3 mL g^{-1}
EST30471-1 $[I^-]_{ini}=10^{-3}$ M	0.35 (0.3-0.4)	0.08 (0.07-0.10)	4 (-9; 13)	0.45 (0.3-0.6)	0.20 (0.18-0.22)	55 (38-64)	0.35 (0.25-0.5)	0.18 (0.15-0.22)	83 (80-88)
EST30471-2 $[I^-]_{ini}=10^{-4}$ M	0.7 (0.55-0.85)	0.25 (0.23-0.30)	64 (47; 94)	0.35 (0.25-0.5)	0.27 (0.24-0.33)	72 (51-106)	0.35 (0.25-0.5)	0.35 (0.27-0.40)	88 (82-101)
EST30471-3 $[I^-]_{ini}=10^{-5}$ M	0.4 (0.3-0.5)	0.25 (0.20-0.28)	64 (38; 85)	0.25 (0.15-0.25)	0.38 (0.37-0.43)	120 (110-150)	0.5 (0.25-0.6)	0.30 (0.25-0.35)	135 (130-150)
EST30471-4 $[I^-]_{ini}=10^{-6}$ M	0.3 (0.25-0.35)	0.18 (0.17-0.25)	47 (38; 60)	0.35 (0.3-0.35)	0.40 (0.33-0.45)	140 (106-166)	0.20 (0.15-0.35)	0.28 (0.18-0.34)	150 124-157)
EST30471-4 $[I^-]_{ini}=10^{-3}$ M	0.35 (0.3-0.35)	0.10 (0.08-0.14)	13 (0; 34)	n-d	n-d	n-d	n-d	n-d	n-d
EST30471-5 with NaS_2O_3 $[I^-]_{ini}=10^{-6}$ M	0.6 (0.5-0.7)	0.18 (0.15-0.22)	38 (21; 60)	0.25 (0.2-0.3)	0.40 (0.35-0.45)	132 (106-157)	0.5 (0.3-0.5)	0.35 (0.30-0.45)	154 (140-166)
EST27337 [a] 484.5-484.8m $[I^-]_{ini}=10^{-3}$ M	0.2 (0.14-0.28)	0.075 (0.07-0.11)	-	n-d	n-d	n-d	n-d	n-d	n-d
EST05641 [b] 476.97-477.35m $[I^-]_{ini}=4.410^{-3}$ M	0.16	0.033	-	n-d	n-d	n-d	n-d	n-d	n-d
EST10425 [c] 454 m 4 samples from EST312 core	0.73	0.098	-	$[I^-]_{ini}=1$ x 10^{-3} M					
	0.67	0.107	4	$[I^-]_{ini}=1$ x 10^{-4} M					
	0.66	0.447	150	$[I^-]_{ini}=5$ x 10^{-6} M					
	0.77	0.261	71	$[I^-]_{ini}=2$ x 10^{-7} M					

[a] data from Savoye *et al.*(2010) on PAC1011 core. [b] data from Descostes *et al.*(2008) on EST205 core. C data from Bazer-Bachi *et al.*2006 [a, b,c] with $[Na_2S_2O_3]=10^{-3}$ mol L^{-1}

Out-diffusion stage

Figure 5 shows the evolution of the ^{125}I total activities measured in the upstream and downstream reservoirs during the out-diffusion stage performed on the cells EST30471-1 (Figure 5(A)) and EST30471-4 (Figure 5 (B)). All the diffusive parameters estimated from this stage were gathered in the Table 4. The values of the effective diffusion coefficient were quite consistent with those derived from the through-diffusion stage. Conversely, the rock capacity factor – α- exhibited higher values than those obtained from the through-diffusion experiments, suggesting that larger amounts of ^{125}I than predicted from the through-diffusion stage had diffused out of the rock samples. In this case, even the cell EST30471-1 in which no sorption was previously observed from the through-diffusion stage showed a significant value of desorption R_D close to 0.05 mL g^{-1}, while the other cells displayed desorption R_D values up to 0.15 mL g^{-1}. A similar trend was previously mentioned by Van Loon *et al.* (2003) and Glaus *et al.* (2008) with rock samples from the Opalinus Clay. They observed no clear iodide uptake from the through-diffusion stage but they measured higher amount of iodide than predicted during the out-diffusion stage. Glaus *et al.* (2008) proposed a reversible accumulation of a minor I species other than I^- in the first layers of the clay sample during the through-diffusion stage.

(B)

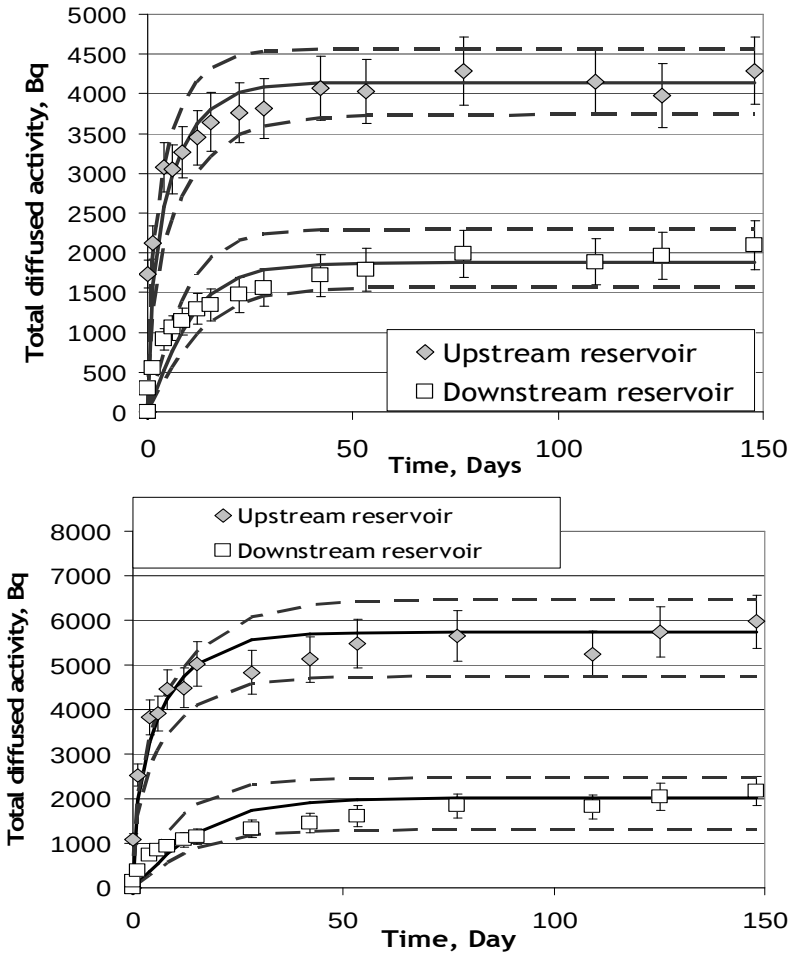

Figure 5: *Evolution of the total diffused activities measured in the upstream and downstream reservoirs during the out-diffusion stage on the cell EST27321-1 (A) and on the cell EST27321-4 (B). Decay corrections were made with respect to the start of the through-diffusion stage.*

3.1.4. Discusion about the iodide behaviour

No sorption was observed from the batch experiments performed, however (i) with a very low water/rock ratio – 4 mL g^{-1}- in order to enhance the sorption extent, if any, and (ii) for up to 106 days. These experimental conditions were chosen as close as possible to those previously used by Bazer-Bachi *et al.*(2006) for their batch experiments, i.e. about 120 days of iodide contact with COx samples and a close water/rock ratio (5 mL g^{-1}). These authors measured R_D values equal to 0.42±0.08 mL g^{-1} at a total iodide concentration of 7 10^{-7} mol L^{-1}. The distinct results obtained can be explained by the use in the Bazer-Bachi et al.'s study of an O_2-free glove box without any CO_2 atmosphere capable of preserving the calco-carbonic equilibria. Therefore, the apparent iodide uptake that Bazer-Bachi *et al.* (2006) measured could likely be an artefact related to a possible co-precipitation of iodide with carbonate minerals.

The values of R_D derived from the through- and out-diffusion experiments are gathered in the Figure 6, as a function of the initial iodide concentration. The results show that (i) the retardation of iodide greatly depends on the iodide concentration and (ii) the iodide uptake would be reversible, with higher amounts of iodide diffusing out of the samples than what predicted from the through-diffusion experiments.

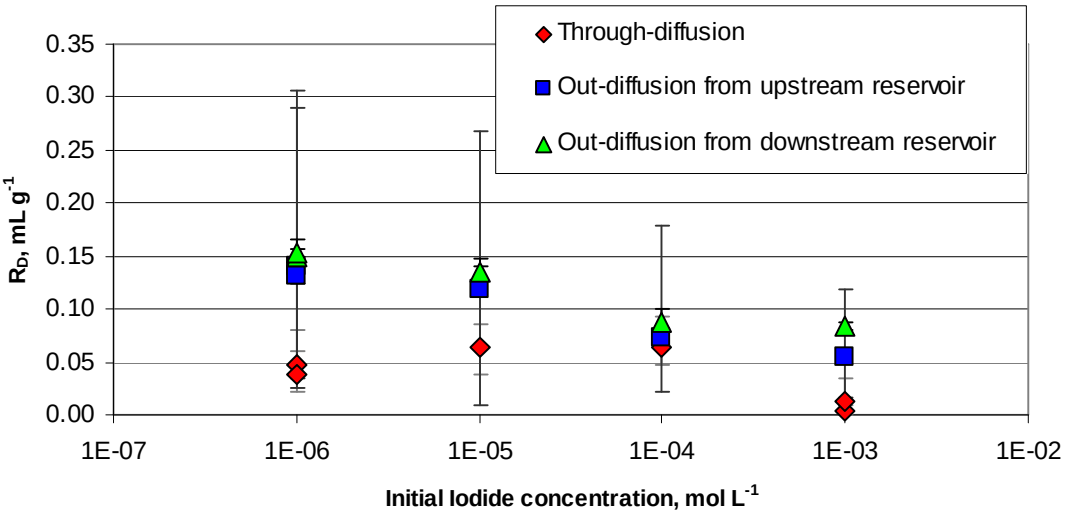

Figure 6: *Comparison of the distribution ratio (R_D) values estimated from the through- and out-diffusion experiments as a function of the initial iodide concentration. Error bars are calculated with uncertainty ranges given in Table 4.*

The concentration-dependent uptake of iodide was often mentioned in literature with sorption evidenced only for iodide concentrations less than or equal to about 10^{-4} mol L^{-1} (Savoye *et al.*, 2006; Bazer-Bachi et al., 2006; Descostes *et al.*, 2008; Wittebroodt *et al.*, 2008; Zhang *et al.*, 2011; Aimoz et al., 2011). Moreover, when desorption was investigated in some of these studies, the iodide uptake was generally found to be largely irreversible. For example, Savoye *et al.* (2006) and Wittebroodt *et al.* (2008) performed out-diffusion experiments with iodide on indurated clay rocks from Tournemire (France) and they found that less than 50% of the iodide initially injected was released, whatever the initial iodide concentration. Descostes *et al.* (2008) observed the same trend from their batch desorption experiments carried out onto COx samples, with less than 5% of the initial iodide desorbed. These authors suspected the natural organic matter (NOM) to be responsible for this irreversible uptake. Indeed, as

previously shown by Reiller *et al.* (2003), Schlegel *et al.* (2006) and Steinberg *et al.* (2008), the iodination of the organic matter leads to the formation of covalent bonds, thus, to an immobilisation of iodine. Such a mechanism is capable of explaining the retardation of the iodide migrating through soils made of relatively fresh and reactive organic matter (See e.g., Zhang *et al.*, 2011, Kaplan *et al.*, 2011). However, more cautions have to be paid for indurated clay rocks, in which NOM are kerogen type, known to be mature and relatively inert (Deniau *et al.*, 2008). Beyond the role played by the NOM, the irreversibility of the iodide uptake observed by Savoye *et al.* (2006), Wittebroodt *et al.* (2008) or Descostes *et al.* (2008) could also have been induced by the same artefact mentioned above: the absence of a controlled partial pressure of CO_2, leading to a disequilibrium towards carbonate minerals, and thus, the co-precipitation of iodide. In the current study, the reversible behaviour of the iodide uptake evidenced from the out-diffusion experiments suggest that the natural organic matter could not be a potential candidate capable of sorbing iodide.

The oxidized pyrite could be another candidate. Indeed, Aimoz *et al.*(2011) showed a concentration-dependent uptake of iodide by this altered mineral even under anoxic conditions (O_2 < 5 ppm) with R_D values ranging from 0.6 to 2 mL g^{-1} for initial iodide concentrations of 10^{-6} and 10^{-11} mol L^{-1} (resp) and R_D value equal to zero for initial iodide concentration of 10^{-3} mol L^{-1}. These authors proposed that iodide sorption would be mainly due to electrostatic outer-sphere complexation of iodide, being bound to Fe(III) oxide-like clusters on the pyrite surface, which were presumably formed by reaction with limited amounts of dissolved oxygen. This mechanism assumed to be reversible (only weak electrostatic outer-sphere complexation), unlike the iodination of NOM, could explained the iodide uptake described in the current study.

Let us now consider the increase of the values of the desorption R_D we obtained from out-diffusion compared to those of the sorption R_D from through-diffusion. Such a difference could be accounted for by a possible kinetically controlled iodide retention, assuming that the longer the iodide contact time with rock, the higher the retention. Note that the through-diffusion method seems less adapted than the out-diffusion one for addressing the kinetic issue. Indeed, on one hand, only does the through-diffusion method enable to estimate the rock capacity factor, i.e., the sorption intensity, from the very beginning of the through-diffusion experiment (Schackelford, 1991), i.e. from the short transient-state (less than 30 days), and thus, before the possible occurrence of some changes of the sorption intensity. However, a more detailed analysis of the ^{125}I flux data (Figure 4) still reveals the existence of some intermediate plateaus before reaching the steady-state, reflecting the possible change with time of the iodide affinity towards the rocks. On the other hand, the out-diffusion method sounds more adapted because launched after a longer period of iodide contact with rock (e.g., after 230 days of through-diffusion, here). Moreover, in this case, when the species has finished diffusing out, the corresponding cumulative activity reaches a plateau, directly related to the rock capacity factor value, and thus, to the desorption R_D (Figure 5).

Among the mechanisms behind the kinetically controlled retention of iodide, one based on the Aimoz *et al.*'s study can be proposed. This mechanism can be related to a slow process of pyrite oxidation that could occur under our nearly anoxic conditions, and could progressively increase the amount of the new reactive phases capable of sorbing iodide, until the iodide desorption. However, this hypothesis fails to take into account the results obtained from the cell EST30471-5, in which was injected a reductive agent ($S_2O_3^{2-}$) to limit oxygen contamination. Indeed, the diffusive behaviour of iodide in this cell was found to be very similar to what observed in the thiosulfate-free cell studied at the same initial iodide concentration (10^{-6} mol L^{-1}). This means that, if the iodide sorption had been related to the oxidation of pyrite, the oxidation could not have occurred throughout the duration of the

experiments but would have taken place before the addition of the reductive agent. Nevertheless, this last statement can also be excluded because of (i) the care paid to limit oxygen entrance (argon-drilled borehole; nearly anoxic conditions throughout the experiments) and (ii) the relative large size of our intact rock samples (1cm) compared to the powered pyrite (< 63µm) used by Aimoz *et al.* (2011), enabling the limitation of the oxygen contamination to the sample surface. Therefore, excluding the slow oxidation of pyrite as a possible candidate led us to assume that the kinetic control could be likely related to the iodide retention mechanism itself, as previously suggested by Bazer-Bachi *et al.* (2006) from their batch experiments performed under oxic conditions but with addition of $S_2O_3^{2-}$. However, no clear mechanism has been yet identified to account for such an increase of the intensity of sorption with the contact time (Savoye *et al.*, submitted).

3.2. Selenium Case

3.2.1. Batch experiments

Figure 7 shows the evolution of the R_D values as a function of time. Even though some artefacts affected the series with the lowest concentration, some tendency can be underlined: the higher the initial selenite concentration, the lower the values of sorption intensity, with R_D values less than 10 mL g^{-1} for $[selenite]_{ini}=10^{-3}$ mol L^{-1} to R_D values more than 200 mL g^{-1} for $[selenite]_{ini}=10^{-6}$ mol L^{-1}. Such an influence of the initial concentration has been already evidenced by other authors (Brugeman *et al.*, 2005).

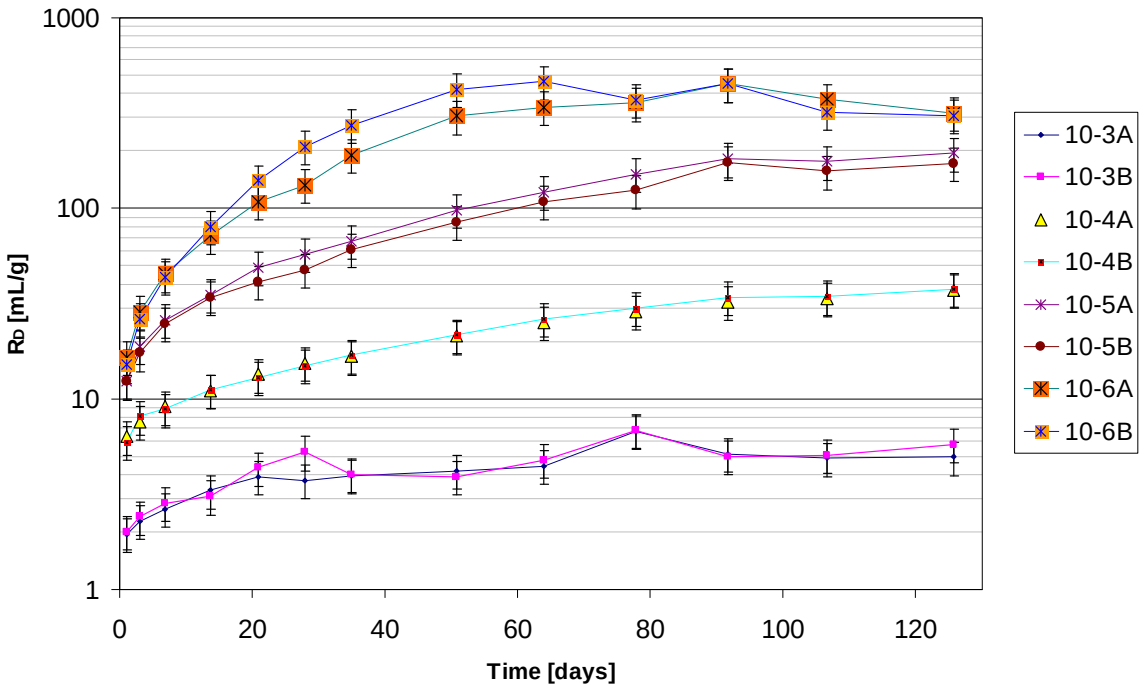

Figure 7: *Evolution as a function of time of the R_D values estimated from Batch Experiments with ^{75}Se and stable selenite at four initial concentrations. R_D values for $[Selenite)_{ini}=10^{-6}$ mol L^{-1} were recalculated by taking into account the blank behaviour.*

3.2.2. Diffusion experiments

Data obtained from the solution monitoring

Figure 8 shows the evolution of the ^{75}Se activity in the upstream reservoir of the cell with the highest initial Se(+IV) content (10^{-3} mol L^{-1}) as a function of time. A clear activity decrease was observed for the 240 days of the experiment. The results of the fractionation indicated that the activity values originating from the active Se(+VI) remained quite constant throughout the duration of the experiment, while the evolution of the total measured activity can clearly be related to the decrease of the ^{75}Se(+IV) activity values (Figure 8).

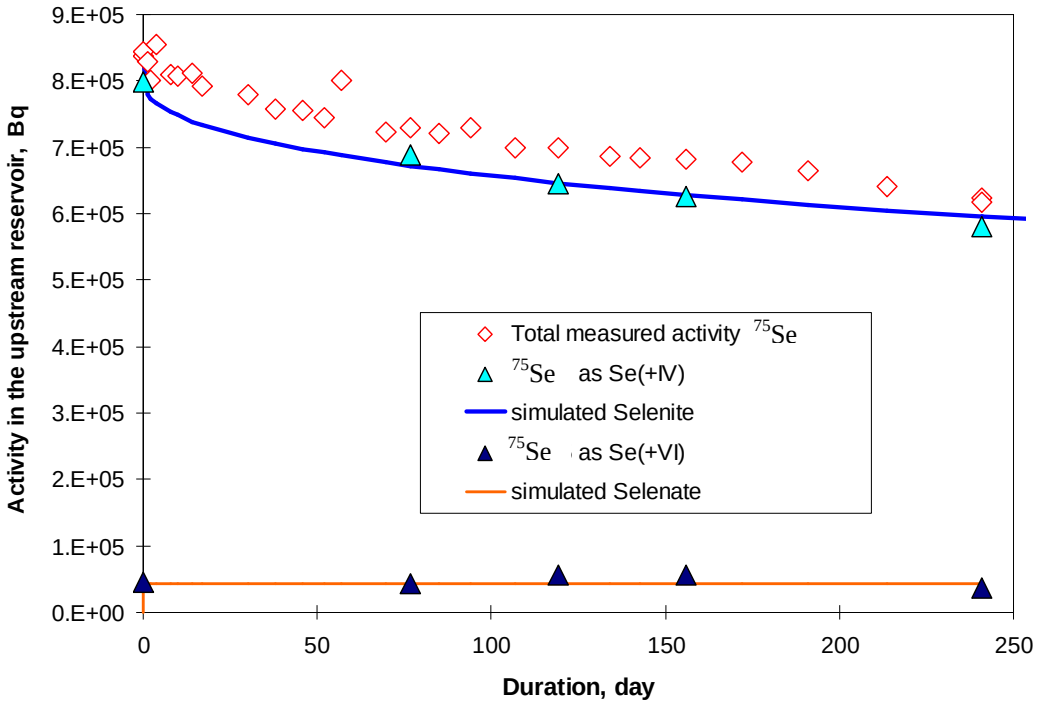

Figure 8: *Evolution of the ^{75}Se activity in the upstream reservoir spiked with Se(+IV)= 10^{-3} mol L^{-1} as a function of time. The curves have been calculated using the corresponding analytical solution using the parameters from Table 5. Closed symbols denote the results of the fractionation. Open symbols denote the activity of total Se determined from the total radioactivity in the samples.*

The normalised incoming fluxes measured in the downstream reservoir for ^{36}Cl and ^{75}Se were reported in Figure 9. Owing to the too low activities measured in this reservoir, which prevented us from applying the fractionation method, only indirect approach was used for estimating the redox state of the selenium having diffused through the rock sample. In fact, some answers can be brought by the fits of the experimental data –Se(+IV) and Se(+VI)- obtained both from the downstream and upstream reservoirs but also from the rock profile (see above) and using the parameters from the Table 8. Indeed, on one hand, fitting the downstream reservoir data, by assuming Se(+IV) as the sole activity contributor can only be achieved, using very low values for the diffusive parameters (De= 1.1 10^{-13} m^2 s^{-1} & α = 0.01), such as those selected by Descostes *et al.*(2008) (see Table 8) and leads to a simulated curve in the upstream reservoir, displaying no decrease and thus, clearly not consistent with the corresponding ^{75}Se(+IV) data. Moreover, taking the parameters used for the fit of the Se(+IV) data determined in the upstream reservoir leads to calculate a very delayed breakthrough curve, clearly not in agreement with the experimental data, as it can be seen in Figure 9. On the other hand, assuming Se(+VI) as the sole activity contributor to the

downstream reservoir allows us to fit well both upstream and downstream data and by means of diffusive parameter values sounding quite consistent (Table 8). Indeed, these values are quite close to those obtained by Descostes *et al.* (2008) for sulphate on sample originating from the same location (Table 8) and De Cannière *et al.* (2010) indicated that Se(+VI) displayed a diffusive behaviour similar to sulphate from diffusive studies on Boom Clay.

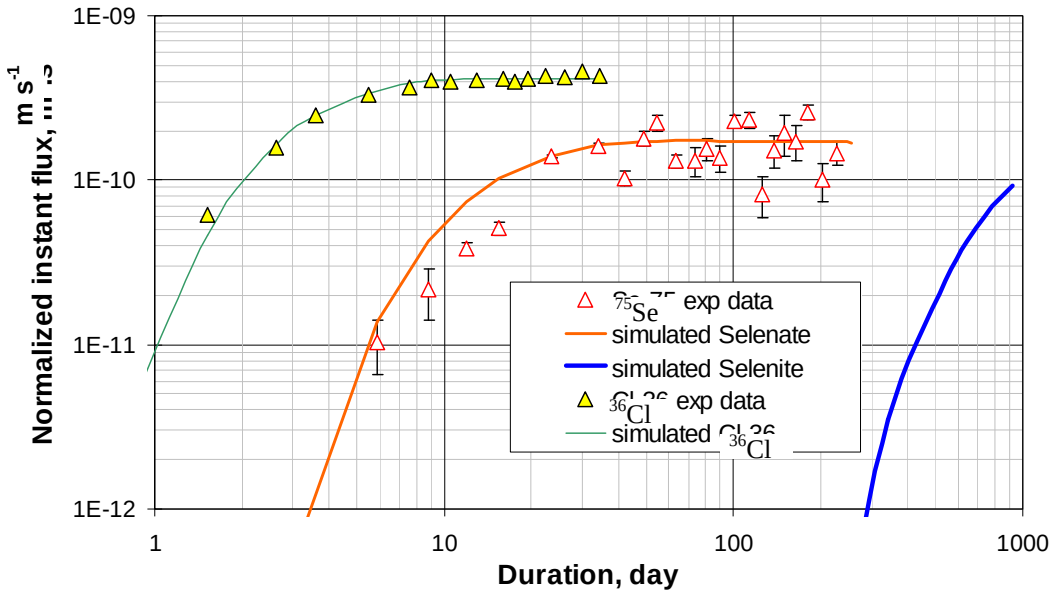

Figure 9: *Normalized instantaneous fluxes of the cell 6 with Se(+IV)=10^{-3}mol L^{-1} for ^{36}Cl and ^{75}Se. The solid curves for the fluxes were calculated using the analytical solutions with the parameters specified in Table 8. Normalized flux is the ratio of instantaneous flux in Bq m^{-2} s^{-1} over the concentration in the upstream reservoir in Bq·m^{-3}.*

Table 8: *Values of rock capacity factor (α), effective diffusion coefficient (De) and distribution ratio (R_D) for the diffusion of HTO, $^{36}Cl^-$, $^{35}SO_4^{2-}$, ^{75}Se(+IV) and ^{75}Se(+VI). Data from Descostes et al. (2008) were obtained on core from borehole EST205. n-d: not determined.*

		HTO	$^{36}Cl^-$	^{75}Se(+IV)	^{75}Se(+VI)	$^{35}SO_4^{2-}$
EST30471-6 480.70–481.70 Se(+IV)= **10^{-3} M**	**α[-]**	0.19	0.07 (0.06-0.08)	28	0.13	n-d
	D_e x 10^{-11} [m^2 s^{-1}]	3.1 (2.8-3.5)	0.48 (0.4-0.55)	0.4	0.2	n-d
	R_D [mL g^{-1}]	0	0	12	0.025	n-d
EST30471-7 480.70–481.70 Se(+IV)= **10^{-6} M**	**α[-]**	0.20 (0.19-0.21)	0.08 (0.07-0.09)	300 to 640	0.09	n-d
	D_e x 10^{-11} [m^2 s^{-1}]	2.7 (2.2-3.5)	0.37 (0.30-0.40)	0.2 to 0.4	0.1	n-d
	R_D [mL g^{-1}]	0	0	100 to 300	0.005	n-d
Descostes *et al.*(2008) EST05641 476.97–477.37	**α[-]**	0.195±0.045	0.065	0.009	n-d	0.31
	D_e x 10^{-12} [m^2 s^{-1}]	22±7	4.6	0.015	n-d	0.2
	R_D [mL g^{-1}]	0	0	0	n-d	0.1

Finally, our experiment permits to shed light on the singular data previously obtained by Descostes *et al.*(2008) with Se(+IV). In fact, the ^{75}Se(+IV) labelled source they used could be suspected to contain a sufficient amount of ^{75}Se(+VI) for diffusing through the sample instead of the more sorbing ^{75}Se(+IV), as described in our study, and thus, for making Descostes *et al.*(2008) give wrong estimates for the diffusive parameters.

The evolution of the selenite concentration as a function of time in the upstream reservoir was given in the Figure 10 for the inactive cell with $[SeO_3^{2-}] = 2 \times 10^{-3}$ M. Even though the scattering is more pronounced than for the radioactive cell, the global tendency is quite the same, given the associated uncertainties.

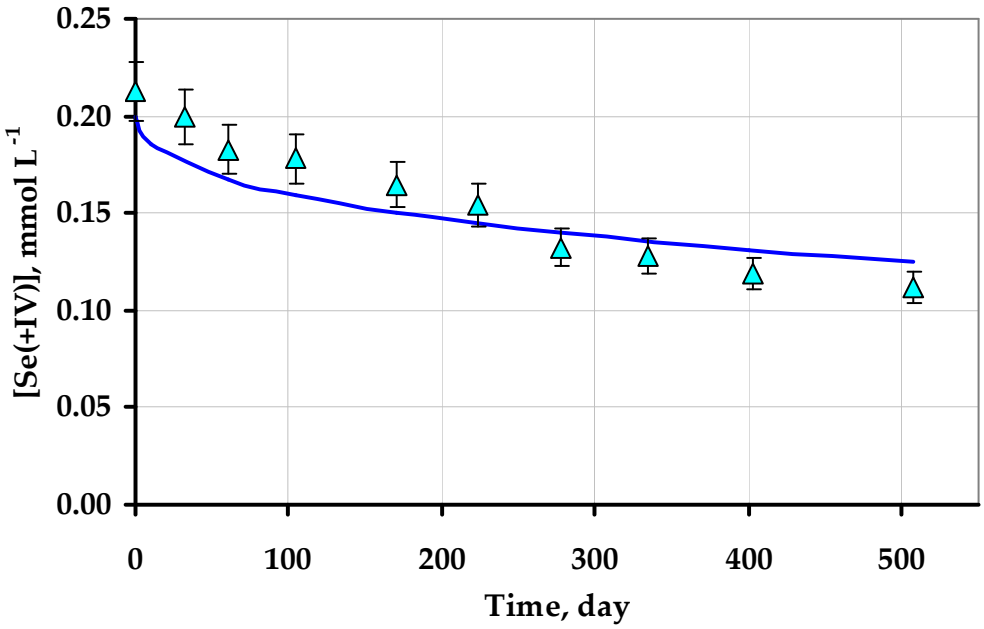

Figure 10: *Evolution of the selenite concentration in the upstream reservoir of inactive cell 8. The curve was calculated using equation (11) with the same parameters than those used for the radioactive cell.*

It is noteworthy that the simulated curve in Figure 10 was calculated with the same parameters as those used for the radioactive cell 6, indicating a relatively good consistency of the data set.
Figure 11 shows the evolution of the ^{75}Se activity in the upstream reservoir as a function of time for the radioactive cell with the lowest initial Se(+IV) content (10^{-6} mol.L^{-1}). A regular decrease is observed for the first 20 days until a rapid drop, and a sort of plateau is reached from the 70th day. The fractionation technique indicates that ^{75}Se(+IV) would be mainly responsible for such an evolution. As already mentioned by Bruggeman *et al.* (2005), Se(+IV) was capable of being undertaken to some reduction phenomena, leading to the precipitation of the more reduced Se forms, and likely kinetics-controlled, as more than 20 days were necessary to reach such a decrease. However, an attempt to roughly fit the first Se(+IV) data (before 20 days) was carried out using parameters given in Table 8.

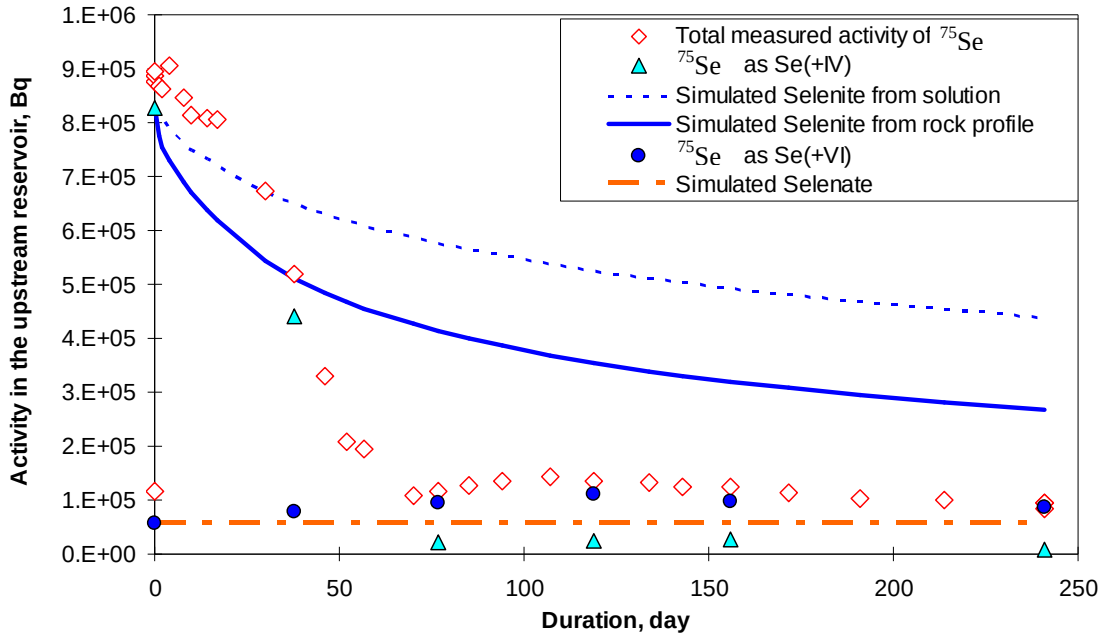

Figure 11: *Evolution of the ^{75}Se activity in the upstream reservoir spiked with Se(+IV)= 10^{-6} mol L^{-1} as a function of time. The curves have been calculated using the corresponding analytical solution using the parameters from Table 8. Closed symbols denote the results of the fractionation. Open symbols denote the activity of total Se determined from the total radioactivity in the samples.*

The normalised incoming fluxes measured in the downstream reservoir for ^{36}Cl and ^{75}Se were reported in Figure 12. Even though the experimental ^{75}Se data were more scattered than those for the cell 6, they were fitted with diffusive parameter values very close to those used for the cell 6, assuming that only $^{75}Se(+VI)$ was involved, as for the cell 6 (Table 8).

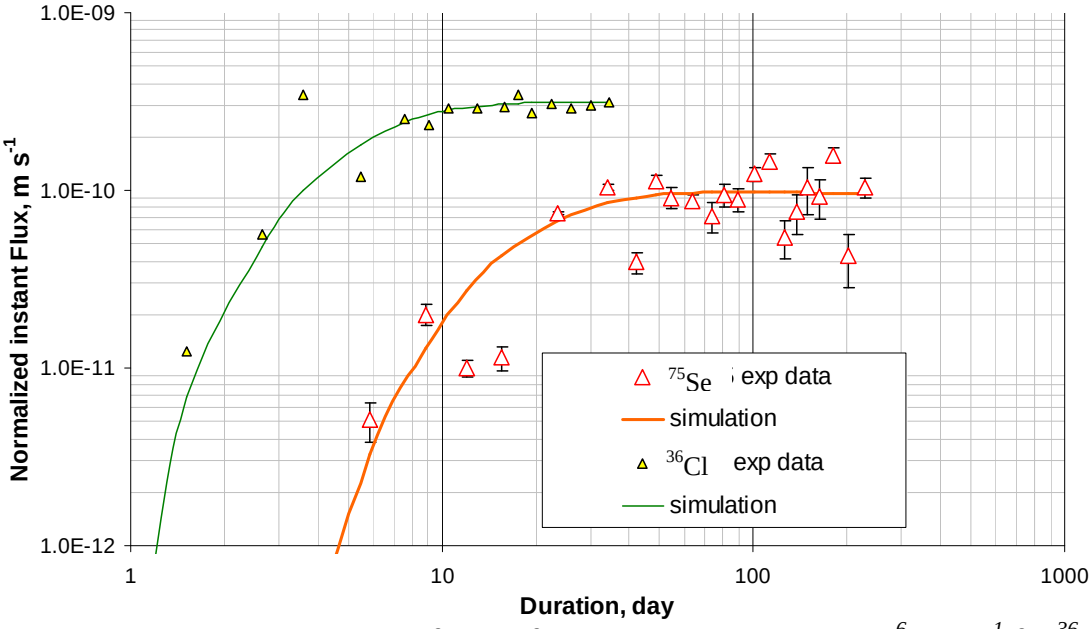

Figure 12: *Normalized instantaneous fluxes of the cell 7 with Se(+IV)=10^{-6} mol L^{-1} for ^{36}Cl and ^{75}Se. The solid curves for the fluxes were calculated using the analytical solutions with the parameters specified in Table 2. Normalized flux is the ratio of instantaneous flux in Bq m^{-2} s^{-1} over the concentration in the upstream reservoir in Bq·m^{-3}.*

Rock profile data

Figure 13 shows the concentration of ^{75}Se (in Bq g^{-1}) as a function of the diffusion distance in the solid for the radioactive cell 6 with the highest selenite concentration. The poor quality of the experimental data fit, especially in the solid, using the equation (15) with *De* equal to 4 x 10 m^2 s^{-1} and α equal to 28 (Table 8), underlines that the global pattern of the ^{75}Se profile cannot be accounted for only by a pure diffusion process with a reversible sorption. Other processes have to be proposed, related, for instance, to some possible redox phenomena.

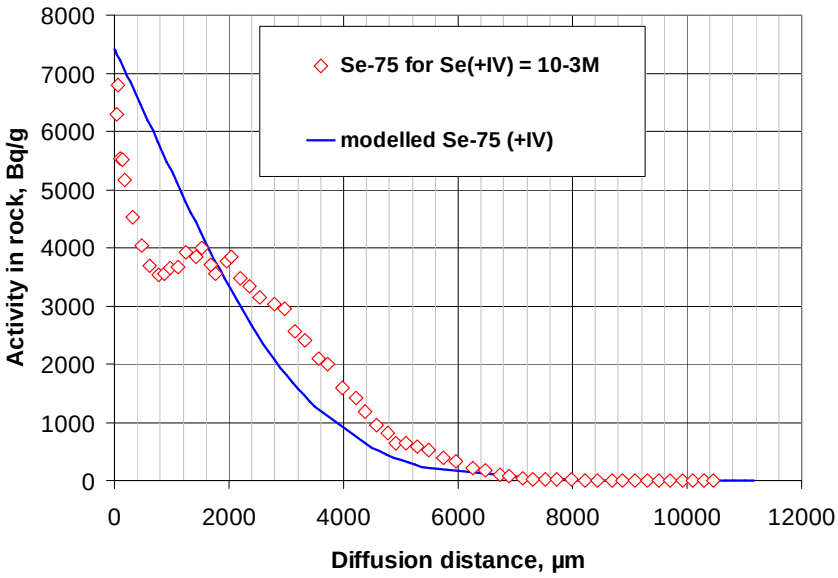

Figure 13: *Concentration profile of ^{75}Se for. Symbols represent experimental data. The curve is the best fit with the parameters given in the Table 8.*

Figure 14 shows the concentration of ^{75}Se (Bq g^{-1}) as a function of the diffusion distance in the cell 7 with the lowest initial selenite concentration (10^{-6}M).

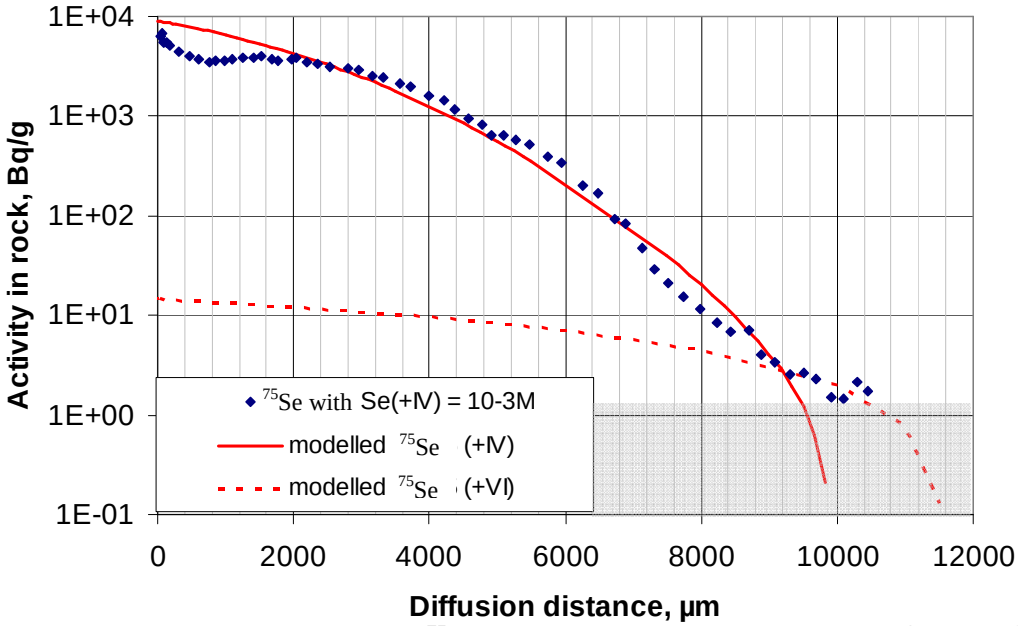

Figure 14: *Concentration profile of ^{75}Se for the cell 1 with Se(+IV)=10^{-3} mol L^{-1}. Symbols represent experimental data. The curves are the best fits with the parameters summarised in Table 8. ^{75}Se activities in the sample beyond a diffusion distance of 10000 µm were below the detection limit. The shaded area denotes concentration ranges around or well below the detection limit.*

The diffusion profile data of the solid sample were fitted using only diffusive parameter values for Se(+IV) (Table 8), the contribution to the activity coming from Se(+VI) being negligible, except maybe in the last centimetre. It is noteworthy that the experimental data are quite scattered even in log scale (Figure 14), making difficult any quantitative estimation of the diffusive parameters. Remind that after 20 days of diffusion, a rapid drop of selenite was observed in the upstream reservoir, meaning that a quite irregular diffusive flux penetrated into the rock.

For the inactive cell 8, based on the studies of Charlet *et al.* (2007) and Frasca (2011), the distribution of the total selenium content was acquired by means of µXRF analyses at an energy of 12800 eV on some selected areas. An example is given in Figure 15 (A) showing a relative homogeneous decrease of the total selenium content from the upstream reservoir interface to the downstream reservoir, with, however, the occurrence of some isolated hot-spots.

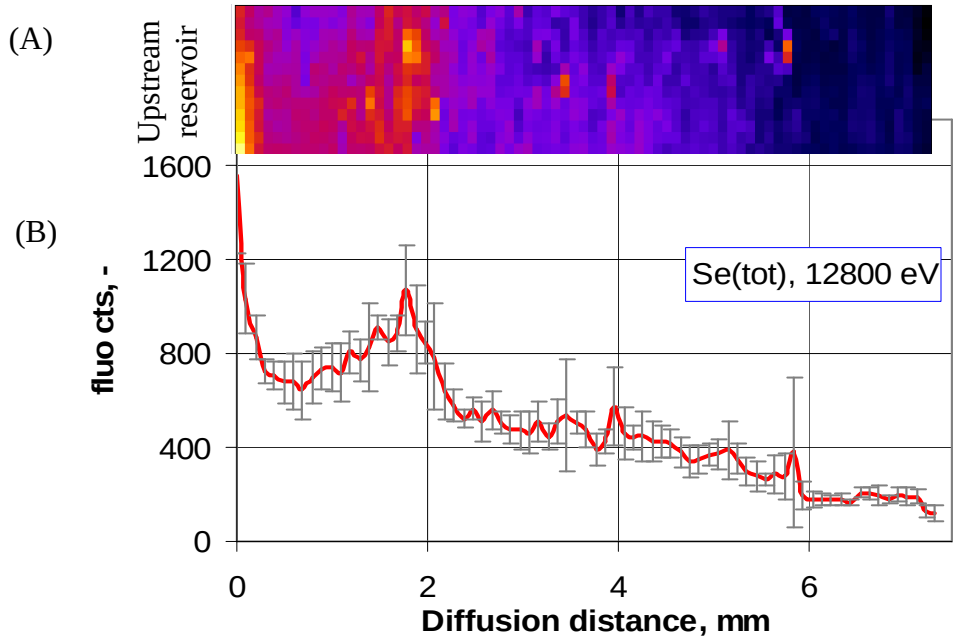

Figure 15: *(A) µXRF mapping of the selenium distribution concentration at 12800 eV. The resolution is for one pixel: 100 µm in X-axis and 50 µm in Y-axis. (B) Average values of total selenium as a function of the diffusion distance. Error bars correspond to the standard deviation.*

The total Selenium profile calculated from this mapping (Figure 15(B)) exhibits a global pattern very similar to the ^{75}Se profile given in Figure 13, with a rapid drop down to 1 mm into the sample, an increase at about 2 mm, followed by a relatively regular decrease.

To identify the evolution of the oxidation state of the selenium species into the sample, Se K-edge XANES spectra were acquired at an energy range from 12645 eV to 12670 eV (Charlet *et al.*, 2007; Frasca, 2011), each 500 µm, on a line from the interface with the upstream reservoir towards the direction of the downstream one (Figure 16). The spectra of the three first samples with respect to the interface are dominated by a strong line at 12664 eV, characteristic of Se(+IV). The spectrum acquired deeper in the profile shows a bigger contribution of a line at 12660 eV, characteristic of more reduced Selenium species, such as Se(0), S(-I) or Se(-II), called here Se(red). This profile demonstrates the occurrence of some

reducing phenomena changing the oxidation state of the selenium during its diffusion through the indurated clay rock sample. The quantification of such a tendency would require a more detailed analysis of the spectrum data set, especially by reconstructing them with some reference spectra.

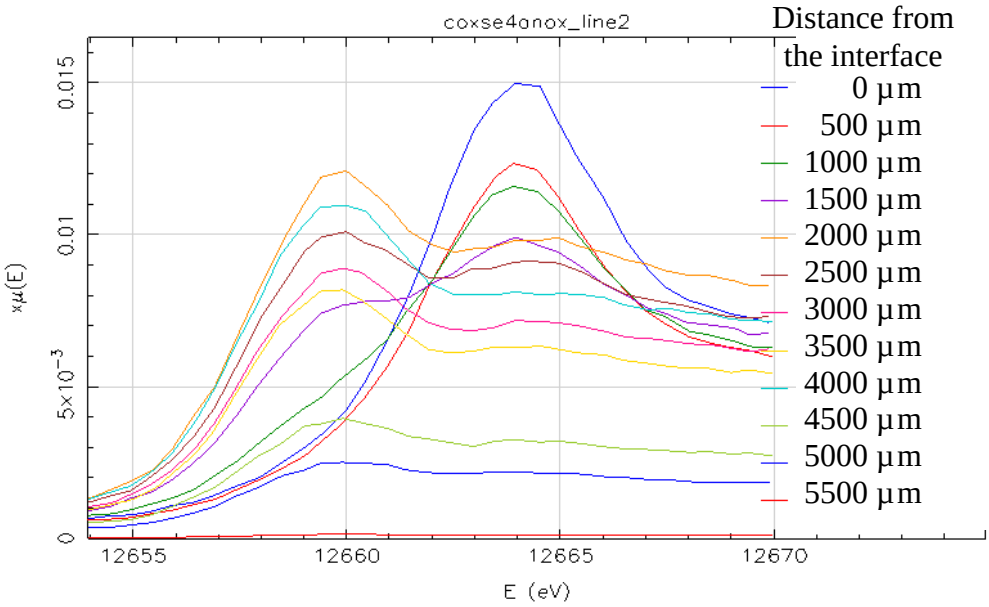

Figure 16: *Selenium K-edge-XANES spectra acquired at an energy range from 12645 eV to 12670 eV, each 500 µm, on a line from the interface with upstream reservoir to the downstream one.*

However, a rough estimate can be obtained, assuming that (i) at the energy equal to 12.664 keV, the contribution from the reduced forms of selenium can be up to the half of the signal intensity acquired at 12.66 keV (Frasca, 2011) and (ii) at the energy equal to 12.660 keV, the contribution from selenite is quite negligible. Therefore, the µXRF mappings carried out at energies equal to 12.660 keV and 12.664 keV allowed us to build a map of the Se(red) from 12.660 keV (Figure 17(A)) and a map of the selenite by deducting the half of the intensity obtained at 12.660 keV to the signal intensity obtained at 12.664 keV (Figure 17(B)).
The Se(red) map exhibits several hot-spots, especially at about 2 mm from the interface (Figure 17(A)), while the selenite map shows a relatively smooth diffusion profile, if though the zone at 2 mm sounds selenite-depleted. Nevertheless, given the very rough approach we used, only the global pattern can be discussed. These tendencies were confirmed when considering the associated profiles built by averaging signals and normalizing by the signal acquired at 12.8 keV, i.e. the total selenium (Figure 17 (D)).

The occurrence of the large Se(red) hot-spot at 2 mm could be explained by some mineralogical heterogeneities, such as the presence of pyrite. To address this issue, the µXRF mapping of Fe acquired for energies ranging from 6.1 to 6.7 keV is presented in Figure 17(C). The distribution of the iron is quite homogeneous over the investigated surface, infirming the assumption given above. However, other Se(red) hot-spots located deeper in the sample can be correlated with some Fe hot-spots (possible occurrence of pyrite).
Another explanation for accounting for the large Se(red) accumulation at 2 mm can be proposed, such as the occurrence of a reducing front located deeper than at the interface because of some redox disturbances related to the solution.

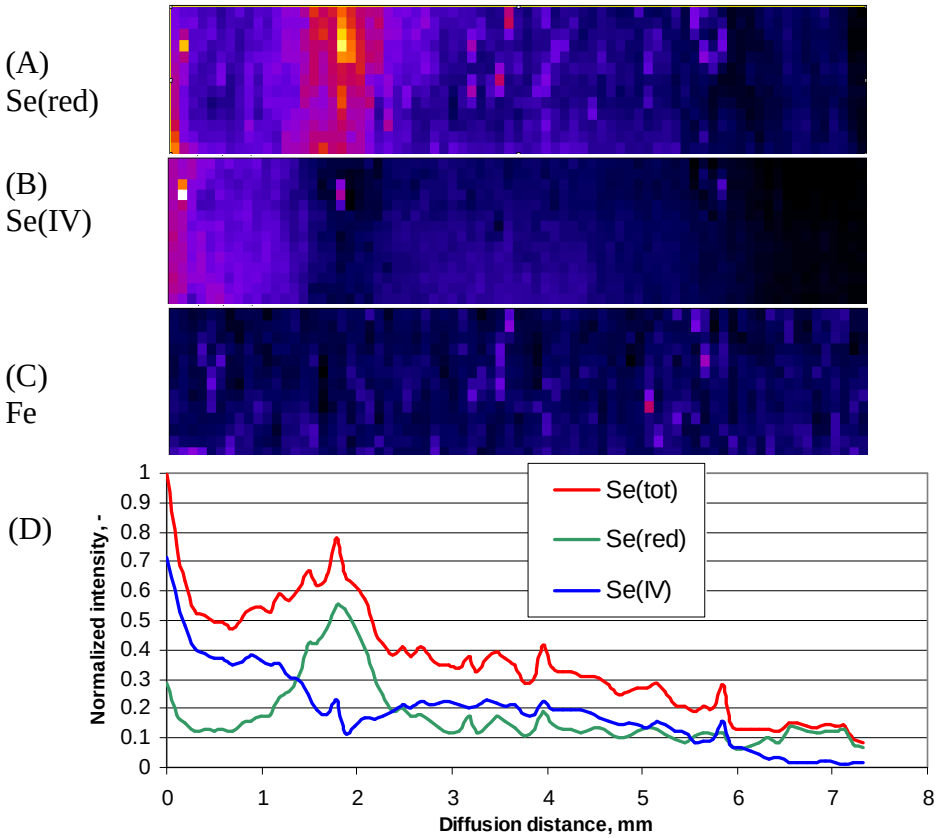

Figure 17: *(A) µXRF mapping of the Se reduced forms acquired at 12.66 keV. (B) µXRF mapping of the selenite from the calculation given in the text. The investigated surface was the same than that in Figure 15. (C) µXRF mapping of Fe acquired at energies ranging from 6.1 to 6.7 keV. The resolution is for one pixel: 100 µm in X-axis and 50 µm in Y-axis. (D) Normalised average values as a function of the diffusion distance.*

3.3. Uranium Case

Figure 18 shows the spectra obtained by time-resolved laser-induced fluorescence spectroscopy (TRLFS) on solutions from the diffusion cell after 106 days of diffusion. The interpretation of these spectra reveals the occurrence of $CaUO_2(CO_3)_3^{2-}$ or/and $Ca_2UO_2(CO_3)_3^{0}$ as the main U(+VI) species.

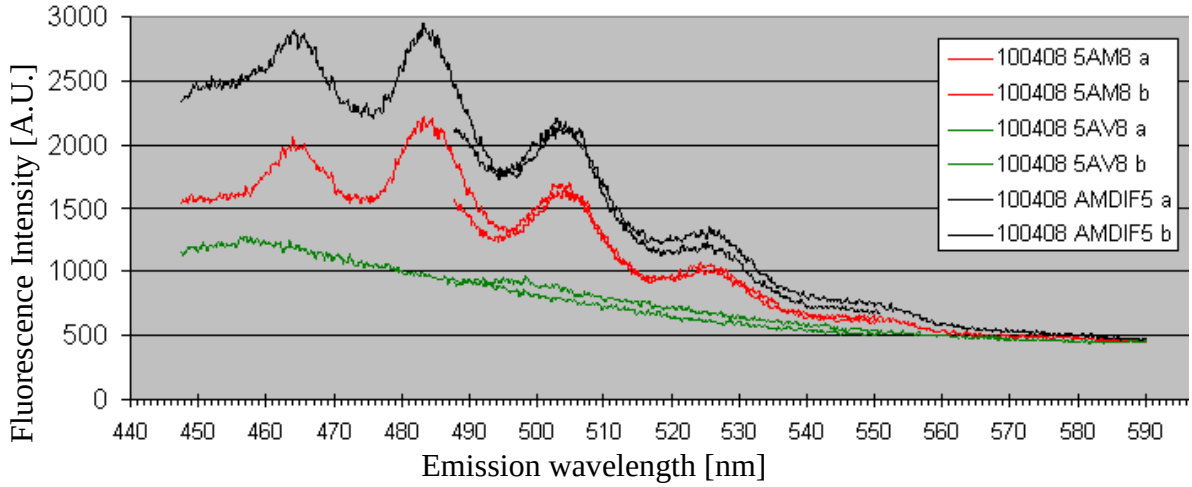

Figure 18: *TRLFS spectra of the downstream, upstream and initially labelled solutions*

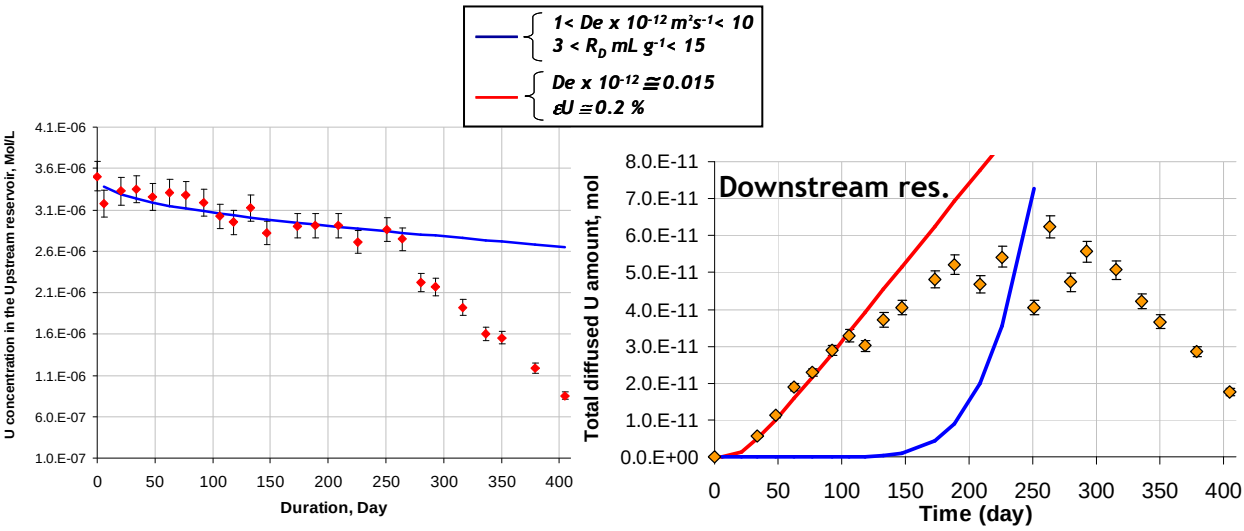

Figure 19: *Comparison of the [U] measured in the upstream (left) and the downstream (right) reservoirs as a function of time.*

As shown in Figure 18, we observed in the downstream reservoir a rapid increase of uranium concentration, suggesting the diffusion of the large anionic molecule, evidenced by TRLFS but only in the high-concentration reservoir, which seems not to be retained onto the rock and to be submitted to a strong steric effect. However, after about 200 days of diffusion, a decrease of U concentration was observed in both reservoirs, likely induced by a reduction/precipitation process, already observed for selenite for the experiments performed with the lowest concentrations ($< 10^{-5}$ mol L^{-1}).

4. Conclusions

From an experimental point of view, this study showed that, even with the drastic conditions we applied, using an O_2-depleted glove-box with N_2/CO_2 atmosphere, we cannot (i) exclude, in some cases, the presence of some bacteria capable of modifying the redox system (e.g., responsible for the [U(VI)] and [Se(IV)] drops in solution) and (ii) guarantee that our physico-chemical conditions were totally similar to those prevailing in-situ.

However, such in-situ conditions seem to be better reproduced by means of the investigations performed with pristine rock samples used for the diffusion set-up compared to powdered samples used for the batch. Indeed, while the batch method was unable to reveal any retention of iodide, the through- and out-diffusion experiments showed a weak but significant uptake. In this case, one cannot exclude that this retention will actually take place in-situ when iodide migrate from the radioactive waste disposal through the claystones. For selenite, the investigations performed especially by XAS onto diffusion samples indicated the co-existence of Se(IV) and more-reduced species all along the profile with some Se(Red) hot-spots. That underlines the complexity of the selenium fate into pristine samples, where the physico-chemical processes of sorption/reduction have to be coupled to the diffusion processes of selenium but also of reducing and oxidising agents. Such a coupling will also have to be taken into account for understanding Uranium diffusing into COx, because of the occurrence of complexes, capable of enhancing its diffusion.

Acknowledgement

The research leading to these results has received funding from the European Union's European Atomic Energy Community's (Euratom) Seventh Framework Programme FP7/2007-2011 under grant agreement n° 212287 (RECOSY project).

Literature cited

Aimoz, L., Curti, E., Mäder, U., 2011. Iodide interaction with natural pyrite. J. Radioanal. Nucl. Chem. 288, 517-524.

Altmann, S., 2008. Geo'chemical research: A key building block for nuclear waste disposal safety cases. J. Contam. Hydrol. 102, 174-179.

Aubriet, H., Humbert, B., Perdicakis, M., 2006. Interaction of U(VI) with pyrite, galena and their mixtures: a theoretical and multitechnique approach. Radiochimica Acta 94, 657-663.

Baur, I, Johnson, C.A., 2003. Sorption of Selenite and Selenate to Cement Minerals. Environ. Sci. Techn. 37, 3442-3447.

Bazer-Bachi, F., Tevissen, E., Descostes, M., Grenut, B., Meier, P., Simonnot, M.-O., Sardin, M., 2006. Characterization of iodide retention on Callovo-Oxfordian argillites and its influence on iodide migration. Phys. Chem. Earth 31, 517-522.

Beaucaire, C., Michelot, J.-L., Savoye, S., Cabrera, J., 2008. Groundwater characterisation and modelling of water-rock interaction in an argillaceous formation (Tournemire, France). Appl. Geochem. 23, 2182-2197.

Bruggeman, C., Maes, A., Vancluysen, J., Vandemussele, P., 2005. Selenite reduction in Boom clay: Effect of FeS2, clay minerals and dissolved organic matter. Environ. Pollut. 137, 209–221.

Charlet, L., Scheinost, A, Tournassat, C., Greneche, J., Gehin A, Fernandez-martinez, A, Coudert, S., Tisserand, D., Brendle J., 2007. Electron transfer at the mineral/water interface: Selenium reduction by ferrous iron sorbed on clay. Geochimica et Cosmochimica Acta 71(23), 5731-5749.

Claret, F., Lerouge, C., Laurioux, T., Bizi, M., Conte, T., Ghestem, J.P., Wille, G., Sato, T., Gaucher, E.C., Giffaut, E., Tournassat, C., 2010. Natural iodine in a clay formation: Implications for iodine fate in geological disposals. Geochim. Cosmochim. Acta 74, 16-29.

Crank, J. The mathematics of diffusion; Oxford Science Publication, New York, 1975.

De Cannière, P., Maes, A., Williams, S., Bruggeman, C., Beauwens, T., Maes, N., and Cowper, M., 2010. Behaviour of selenium in Boom Clay. Work performed under contract: SCK•CEN ref:CO 90 01 1467.01 1467 RP.W&D.037 – NIROND ref: CCHO2004/00/00 DS251-A44/2.1.

Deniau, I., Devol-Brown, I., Derenne, S., Behar, F., Largeau, C., 2008. Comparison of the bulk geochemical features and thermal reactivity of kerogens from Mol (Boom Clay), Bure (Callovo–Oxfordian argillite) and Tournemire (Toarcian shales) underground research laboratories. Sci. Tot. Environ. 389, 475 – 485.

Descostes, M., Blin, V., Bazer-Bachi, F., Meier, P., Grenut, B., Radwan, J., Schlegel, M., Buschaert, S., Coelho, D., Tevissen, E., 2008. Diffusion of anionic species in Callovo-Oxfordian argillites and Oxfordian limestones (Meuse/Haute-Marne, France). Appl. Geochem. 23, 655-677.

Descostes, M., Tevissen, E., 2004. Definition of an equilibration protocol for batch experiments on Callovo-Oxfordian argillite. Phys. Chem. Earth. 29, 79-90.

Frasca B., 2011. Migration de l'iode et du sélénium au travers de roches argileuses. Thèse de L'Université Paris-Sud, Orsay.

Fuhrmann, M., Bajt, S., Schoonen, M.A.A., 1998. Sorption of iodine on minerals investigated by X-ray adsorption near edge structure (XANES) and 125I- tracer sorption experiment. Appl. Geochem. 13, 127-141.

Jacquier, P., Ly, J., Meier, P., 2001. Adsorption of radioelements on mixtures of minerals — experimental study. Applied Geochemistry 16(1), 85-93.

Gaucher, E., Robelin, C., Matray, J.-M., Négrel, G., Gros, Y., Heitz, J.-F., Vinsot, A., Rebours, H., Cassagnabère, A., Bouchet, A., 2004. ANDRA underground research laboratory:

interpretation of the mineralogical and geochemical data acquired in the Callovian–Oxfordian formation by investigative drilling. J. Phys. Chem. Earth 29, 55–77.

Gimmi, T., Kosakowski, G., 2011How mobile are sorbed cations in clays and clay rocks? Environ. Sci. Techno. 45, 1443-1449.

Glaus, M.A., Müller, W., Van Loon, L.R., 2008. Diffusion of iodide and iodate through Opalinus Clay: Monitoring of the redox state using an anion chromatographic technique. Appl. Geochem. 23, 3612-3619.

Grambow, B., 2008. Mobile fission and activation products in nuclear waste disposal. J. Contam. Hydrol. 102, 180-186.

Jakob, A., Sarott, F.-A., Spieler, P., 1999. Diffusion and sorption on hardened cement pastes – experiments and modelling results. PSI Bericht 99-05, Paul Scherrer Institut,Villigen, Switzerland.
http://www.nagra.ch/documents/database/dokumente/$default/Default%20Folder/Publikationen/NTBs%201994-2000/e_ntb99-06.pdf

Kaplan, D. I., Roberts, K. A., Schwehr, K. A., Lilley, M. S., Brinkmeyer, R., Denham, M. E., DiPrete, D., Li, H.-P., Powell, B. A., Xu, C., Yeager, C. M., Zhang, S. J., Santschi, P. H., 2011. Evaluation of a radioiodine plume increasing in concentration at the Savannah River Site. Environ. Sci. Technol. 45, 489–495.

Motellier, S., Devol-Brown, I., Savoye, S., Thoby, D., Alberto, J.-C., 2007. Evaluation of tritiated water diffusion through the Toarcian clayey formation of the Tournemire experimental site (France). J. Contam. Hydrol. 94, 99-108.

Reiller, P., Moulin, V., 2003. Influence of organic matter in the prediction of iodine migration in natural environment. Mater. Res. Soc. Symp. Proc. 757, 565–570.

Savoye, S., Michelot, J.-L., Wittebroodt, C., 2006. Evaluation of the reversibility of iodide uptake by argillaceous rocks by the radial diffusion method. Radiochim. Acta 94, 699-704.

Savoye, S., Page, J., Puente, C., Imbert, C., Coelho, D., 2010. A new experimental approach for studying diffusion through an intact and unsaturated medium: A case study with Callovo-Oxfordian argillite. Environ. Sci. Technol. 44, 3698-3704.

Savoye, S., Goutelard, F., Beaucaire, C., Charles, Y., Fayette, A., Herbette, M., Larabi, Y., Coelho., D., 2011. Effect of temperature on the containment properties of argillaceous rocks: The case study of Callovo–Oxfordian claystones. J. Contam. Hydrol. 125, 102-112.

Savoye, S., Beaucaire, C., Fayette, A., Herbette, M., Coelho D., 2012 Mobility of caesium through the Callovo-Oxfordian claystones under partially saturated conditions Environ. Sci. Techno. doi.org/10.1021/es2037433.

Savoye, S., Frasca, B., Grenut, B., Fayette, A. How mobile is iodide in the Callovo-Oxfordian claystones under experimental conditions close to the in situ ones? Submitted to Journal of Contaminant Hydrology.

Schackelford, C.D., 1991. Laboratory diffusion testing for waste disposal: A review. J. Contam. Hydrol. 7, 177-217.

Schlegel, M. L., Reiller, P., Mercier-Bion, F., Barre, N., Moulin, V. 2006. Molecular environment of iodine in naturally iodinated humic substances: Insight from X-ray absorption spectroscopy. Geochim. Cosmochim. Acta 70, 5536–5551.

Steinberg, S. M., Kimble, G. M., Schmett, G. T., Emerson, M. F., Turner, M. R., 2008. Abiotic reaction of iodate with sphagnum peat and other natural organic matter. J. Radioanal. Nucl. Chem. 27, 185–191.

Tournassat, C., Gaucher, E.C., Fattahi, M., Grambow, B., 2007. On the mobility and potential retention of iodine in the Callovo-Oxfordian formation. Phys. Chem. Earth 32, 539-551.

van Brakel, J., Heertjes, P. M., 1974. Analysis of diffusion in macroporous media in terms of a porosity, a tortuosity and a constrictivity factor. Int. J. Heat Mass Transfer 17, 1093–1103.

Van Loon, L.R., Soler, J.M., Jakob, A., Bradbury, M.H., 2003. Effect of confining pressure on the diffusion of HTO, 36Cl- and 125I- in a layered argillaceous rock (Opalinus Clay): diffusion perpendicular to the fabric. Appl. Geochem. 18, 1653-1662.

Van Loon, L.R., Eikenberg, J., 2005. A high-resolution abrasive method for determining diffusion profiles of sorbing radionuclides in dense argillaceous rocks. Appl. Rad. Isot. 63, 11–21.

Vinsot, A., Mettler, S., Wechner, S., 2007. In situ characterization of the Callovo-Oxfordian pore water composition. Phys. Chem. Earth 33, 75-86.

Wittebroodt, C., Savoye, S., Gouze, P., 2008. Influence of initial iodide concentration on the iodide uptake by the argillite of Tournemire. Phys. Chem. Earth 33, 943-948.

Wittebroodt, C., Savoye, S., Frasca, B., Gouze, P., Michelot, J.-L., 2012. Diffusion of HTO, 36Cl- and 125I- in Upper Toarcian argillite samples from Tournemire: Effects of initial iodide concentration and ionic strength. Appl. Geochem., doi:10.1016/j.apgeochem.2011.12.017.

Zhang, S., Du, J., Xi, C., Schwehr, K.A., Ho, Y.-F., Li, H.-P., Roberts, K.A., Kaplan, D.I., Brinkmeyer, R., Yeager, C.M., Chang, H., Santschi, P.H, 2011. Concentration-dependent mobility, retardation, and speciation of iodine in surface sediment from the Savannah River Site. Environ. Sci. Technol. 45, 5543-5549.